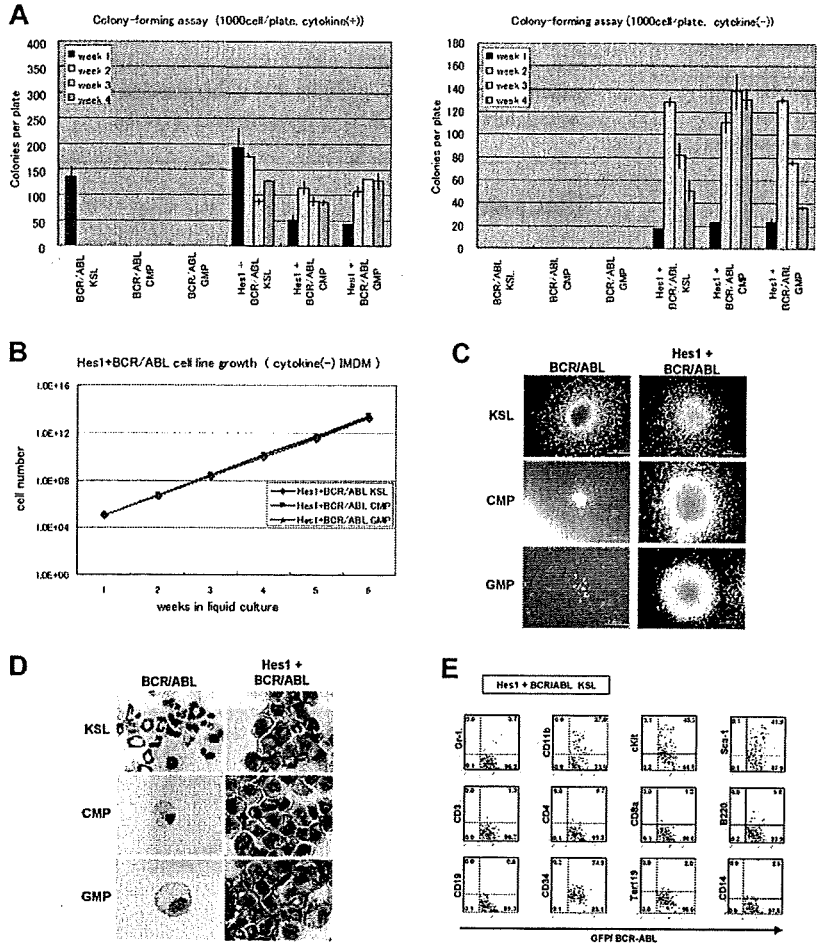

Figure 2. Hes1- and BCR-ABL-transduced KSLs, CMPs, or GMPs were immortalized independently of IL-3. (A) Colony-forming assay of KSLs, CMPs, and GMPs transduced with BCR-ABL alone or Hes1 and BCR-ABL, cultured in methylcellulose with or without cytokine cocktail containing SCF, TPO, IL-3, and IL-6. Hes1$^+$BCR-ABL$^+$ cells could be serially replated more than 4 times both with or without cytokines. In contrast, whereas KSLs, but not CMPs or GMPs, transduced with BCR-ABL alone, formed colonies in the presence of cytokines, neither KSLs, nor CMPs, nor GMPs formed colonies without cytokine supplementation. Bars represent the number of colonies obtained per 10^3 cells after each round of plating in methylcellulose. A representative result from 3 independent and reproducible experiments is shown. Error bars represent the SD from duplicate cultures. (B) Sustained growth of Hes1$^+$BCR-ABL$^+$ cells in liquid culture without cytokine supplementation. The numbers of cells were determined every 7 days by trypan blue staining, and 10^5 cells per well were seeded into a 6-well plate. Liquid culture was reproducibly continued for more than 6 months. (C) Typical colonies derived from KSLs, CMPs, and GMPs transduced with BCR-ABL alone (left panels) or BCR-ABL and Hes1 (right panels) in the presence of SCF, TPO, IL-3, and IL-6. Images were obtained with an IX70 microscope and a DP70 camera (Olympus); an objective lens, UPlanFI (Olympus); original magnification ×100. (D) Giemsa staining of Hes1$^+$BCR-ABL$^+$ KSLs, CMPs, and GMPs. Images were obtained with a BX51 microscope and a DP12 camera (Olympus); an objective lens, UPlanFI (Olympus); original magnification ×1000. (E) Flow-cytometric analysis of Hes1$^+$BCR-ABL$^+$ KSLs cultured in methylcellulose supplemented with SCF, TPO, IL-3, and IL-6. The dot plots represent Gr-1, CD11b, c-Kit, Sca-1, CD3, CD4, CD8a, B220, CD19, CD34, Ter119, and CD14 labeled with a corresponding PE-conjugated monoclonal antibody versus expression of GFP/BCR-ABL. Hes1$^+$BCR-ABL$^+$ CMPs and GMPs showed a similar expression pattern (supplemental Figure 2C-D). The analyzed cells were GFP and NGFR sorted at 48 to 60 hours from the initiation of BCR-ABL- or Hes1+BCR-ABL transduction and cultured for the following lengths of time before the analysis: (A) 0 days, (B) 4 weeks, (C) 1 week, (D) 1 week, and (E) 1 week.

after sublethal irradiation. The numbers of cells injected varied among experiments, ranging from 17×10^2 to 15×10^4, because of the difference in sorting efficiencies. All the mice receiving transplantations rapidly developed fatal AML/CML in blast crisis-like disease with no significant difference in latency, ranging between 18 and 39 days after the transplantation ($P < .867$) (Figure 4A). The tissue distribution of the disease was virtually the same among mice receiving KSLs, CMPs, and GMPs; they invariably demonstrated marked hepatosplenomegaly and lung hemorrhage resulting from infiltration of leukemic cells (Figure 4B). Expression of Hes1 and BCR-ABL in the spleen cells of recipient mice was confirmed by Western blot analysis (supplemental Figure 4B).

The morphology of bone marrow demonstrated increased myeloid blasts (Figure 4C), and the histology of spleen, liver, and lungs demonstrated extensive infiltration of leukemic cells (Figure 4D). The percentages of the blasts ranged between 28% and 55% of all nucleated bone marrow cells (mean, 36.5%) of the mice receiving Hes1- and BCR-ABL-transduced KSLs, CMPs, and GMPs. In contrast, the percentages of bone marrow blasts in the recipient mice receiving BCR-ABL-transduced KSLs were only 6% to 7% (Figure 5A). White blood cell counts in the peripheral blood of recipients with Hes1$^+$BCR-ABL$^+$ KSLs, CMPs, and GMPs were $2.4 \times 10^4/\mu L$ to $67.9 \times 10^4/\mu L$ (mean, $17.8 \times 10^4/\mu L$), whereas those with BCR-ABL-transduced KSLs showed moderate leukocytosis ranging between $2.9 \times 10^4/\mu L$ and $3.8 \times 10^4/\mu L$ (Figure 5B). The surface marker profiles of the bone marrow cells from the recipients with Hes1$^+$BCR-ABL$^+$ cells expressed CD11b and Gr-1 at high levels, whereas they expressed c-Kit, Sca-1, and CD34 at intermediate levels (Figure 5C; supplemental Figure 5A-B), irrespective of whether they were derived from KSLs, CMPs, or GMPs (supplemental Figure 5C).

The long-term self-renewal properties of the leukemic cells derived from Hes1- and BCR-ABL-transduced CMPs or GMPs were tested by transplantation into secondary recipients; 0.1 to 5×10^6 total bone marrow cells were injected into the tail veins of sublethally irradiated mice. All recipient mice transplanted with more than 10^5 Hes1$^+$ cells from bone marrow developed fatal AML/CML in blast crisis-like disease with latencies of between 18 and 75 days (supplemental Figure 4C). The disease was almost identical with the primary disease (data not shown).

Hes1 expression is elevated in a substantial subset of human CML blast crisis samples

The results presented from the mouse model experiments suggest a potential link between deregulated expression of Hes1 and human CML in blast crisis. We measured the Hes1 mRNA by real-time RT-PCR in 11 peripheral blood, 1 cerebrospinal fluid, and 8 bone marrow samples from CML in blast crisis patients; 19 bone marrow samples from CML in chronic phase patients; and 10 bone marrow samples from normal subjects. In 8 of 20 CML in blast crisis samples, we found that Hes1 mRNA levels were elevated by more than 4 times the average of normal bone marrow samples (Figure

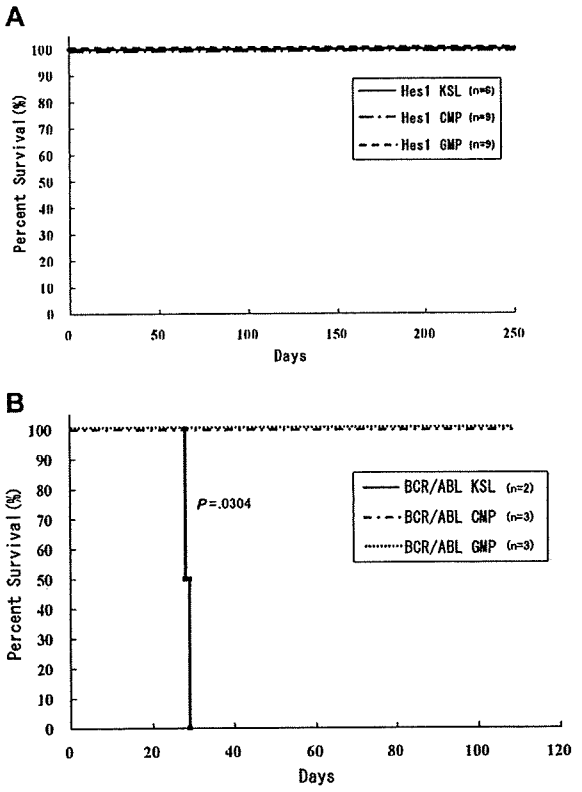

Figure 3. Mice transplanted with Hes1-transduced KSLs, CMPs, and GMPs were kept healthy. (A) Survival curves for mice injected with Hes1-transduced progenitors. No mice showed any signs of MPN for more than 250 days from transplantation. Data were analyzed by the Kaplan-Meier method. The numbers of transplanted mice are shown. Three independent experiments were performed. (B) Survival curves for mice injected with BCR-ABL-transduced progenitors. Mice transplanted with BCR-ABL-transduced KSLs developed fatal MPN within 30 days after transplantation, whereas mice transplanted with BCR-ABL-transduced CMPs or GMPs showed no evidence of disease when killed between 130 and 200 days after transplantation. Data were analyzed using the log-rank test. The 2 independent experiments were performed, and the total numbers of transplanted mice are shown.

6A). Interestingly, all but one of their phenotypes were myeloid, and 5 of 12 samples in which Hes1 mRNA levels were not elevated were derived from patients with B-cell lineage lymphoid crisis. On the other hand, the average of Hes1 mRNA levels in CML in chronic phase samples seemed to be lower than that of the normal bone marrow samples, with no sample exceeding twice the average. Clinical data of 20 patients with CML in blast crisis are shown in Table 1. The correlation coefficient between the blast percentage and the Hes1 mRNA level was −0.395, indicating that the elevated Hes1 expression level was independent of the increase in the blast percentage.

To investigate the role of Hes1 in CML blast crisis, we measured the Hes1 mRNA by real-time RT-PCR in 5 human cell lines (K-562,[27] JK-1,[28] KCL-22,[29] TS9:22,[30] and JURL-MK1[31]), which were derived from CML in blast crisis. We found that, in 3 of 5 CML blast crisis cell lines, Hes1 mRNA levels were elevated compared with the normal bone marrow sample (Figure 6B). We transduced a dominant-negative Hes1 (dnHes1) lacking a C-terminal WRPW domain via retrovirus vector into the 3 cell lines (K-562, TS9:22, and JURL-MK1) in which Hes1 mRNA levels were elevated. Indeed, in 2 of these 3 cell lines, proliferation was significantly suppressed by transduction of dnHes1 (Figure 6C). The repression of C/EBP-α by Hes1 was also observed in Hes1-transduced KSLs, CMPs, and GMPs compared with control vector-transduced KSLs, CMPs, and GMPs (Figure 6D). When C/EBP-α retrovirus vector was transduced to Hes1-transduced KSLs, CMPs, and GMPs, all of these cells differentiated to segmented neutrophils, suggesting that the expression of C/EBP-α reversed the function of Hes1 (supplemental Figure 6).

Discussion

In the present study, we demonstrated that retroviral transduction of Hes1 readily immortalizes myeloid progenitors at various stages.

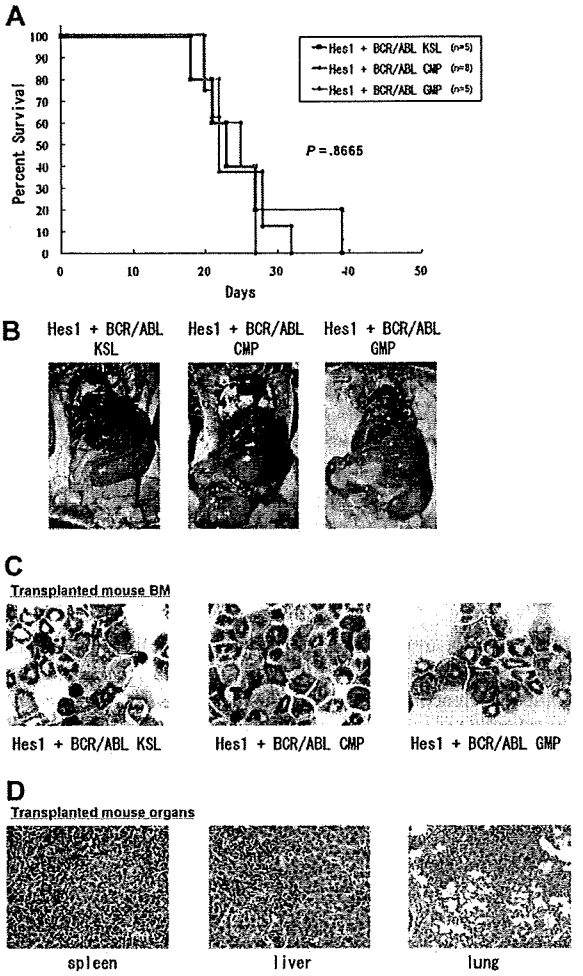

Figure 4. CMPs and GMPs transduced with the combination of Hes1 and BCR-ABL rapidly induced AML/blast crisis of CML. (A) Survival curves of mice. KSLs (n = 5), CMPs (n = 8), and GMPs (n = 5) transduced with the combination of Hes1 and BCR-ABL developed fatal AML/CML in blast crisis-like disease within 18 to 39 days, 20 to 32 days, and 20 to 27 days, respectively. Numbers of injected cells ranged 17×10^2 to 2.6×10^4 for KSLs, 5.5×10^4 to 15×10^4 for CMPs, and 4.0×10^4 to 13.8×10^4 for GMPs. There was no significant difference in latency of penetrance ($P < .867$). Statistical differences were determined using the log-rank test. Three independent experiments were performed, and the total numbers of transplanted mice are shown. (B) Tissue distribution of the leukemic cells. Mice transplanted with KSLs, CMPs, and GMPs transduced with the combination of Hes1 and BCR-ABL invariably demonstrated marked hepatosplenomegaly and lung hemorrhage, both resulting from infiltration of leukemic cells. (C) The morphology of bone marrow cells from representative recipient mice. Increased myeloid blasts were seen with no significant difference among KSLs, CMPs, and GMPs. (D) Histology of spleen, liver, and lungs from representative mice receiving Hes1$^+$BCR-ABL$^+$ GMPs. Vast infiltration of leukemic cells is seen. There were no differences in the histology among mice receiving Hes1$^+$BCR-ABL$^+$ KSLs, CMPs, and GMPs.

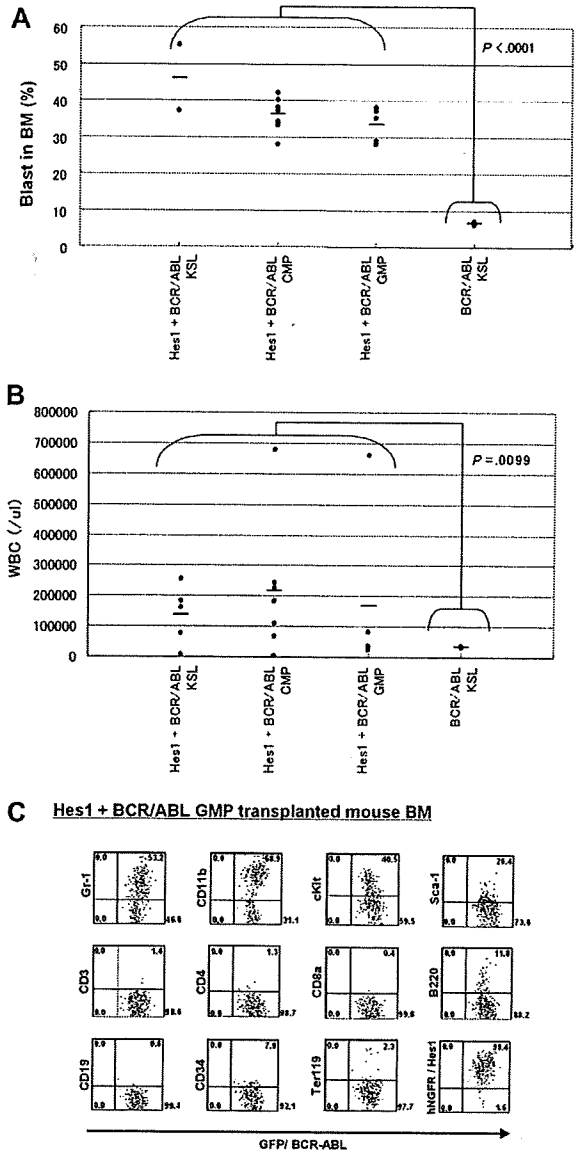

Figure 5. Comparisons of blast percentages in the bone marrow and peripheral blood leukocyte counts between mice receiving KSLs transduced with BCR-ABL alone and those receiving KSLs, CMPs, and GMPs transduced with the combination of Hes1 and BCR-ABL. (A) Blast ratios in the bone marrow. The mean blast ratios in all nucleated bone marrow cells were 6.5% ± 0.7% and 36.5% ± 6.9% in mice receiving KSLs transduced with BCR-ABL alone and in those receiving KSLs, CMPs, and GMPs transduced with the combination of Hes1 and BCR-ABL, respectively. The difference was statistically significant by the 2-sample *t* test with Welch correction ($P < .001$). (B) Peripheral white blood cell counts (WBCs). WBCs were $3.4 \pm 0.6 \times 10^4/\mu L$ and $17.8 \pm 20.3 \times 10^4/\mu L$ in mice receiving KSLs transduced with BCR-ABL alone and in those receiving KSLs, CMPs, and GMPs transduced with the combination of Hes1 and BCR-ABL, respectively. The difference was statistically significant by the 2-sample *t* test with Welch correction ($P < .001$). (C) Flow-cytometric analysis of bone marrow cells from mice receiving GMPs transduced with the combination of Hes1 and BCR-ABL. The dot plots represent Gr-1, CD11b, c-Kit, Sca-1, CD3, CD4, CD8a, B220, CD19, CD34, Ter119, and NGFR labeled with the corresponding PE-conjugated monoclonal antibody versus expression of GFP/BCR-ABL. NGFR is a marker of Hes1, and GFP is a marker of BCR-ABL transduction. The bone marrow cells derived from mice receiving KSLs or CMPs transduced with the combination of Hes1 and BCR-ABL showed essentially the same pattern (supplemental Figure 5A-B).

Moreover, when BCR-ABL is transduced together, Hes1 tranforms differentiated myeloid progenitors, such as CMPs and GMPs, in addition to hematopoietic stem cell-rich population, such as KSLs, to AML/CML in blast crisis-like cells, rapidly killing recipient mice. This result is in sharp contrast to the fact that a hematopoietic stem cell-containing population is required for BCR-ABL to cause MPN-like disease.

Hes1 is known as an effector molecule functioning downstream of Notch signaling. The activating mutations of the extracellular heterodimerization domain and/or the C-terminal PEST domain of Notch1 have been identified in approximately 50% of human T-cell acute lymphoblastic leukemias.[10,32] We have recently identified gain-of-function mutations of *Notch2* in conjunction with increased copy numbers of the mutation-carrying *Notch2* allele in a subset of B-cell lymphomas.[11] A possible association between deregulated Notch signaling is also reported in Hodgkin lymphoma, anaplastic large cell lymphoma, small-cell lung cancer, and prostate adenocarcinoma, etc.[33] Regarding myeloid malignancies, however, only one paper reports the identification of the activating mutation of Notch1 in 1 of 12 human AML samples.[34] Given that Notch signaling is among the strongest inducers of T-cell lineage commitment[12,13] and that increased Notch signaling could block myeloid lineage commitment,[15] deregulated Notch signaling might antagonize, rather than promote, the development of myeloid malignancies. However, Hes1 does not necessarily represent Notch signaling. Indeed, other extracellular signaling, such as Sonic Hedgehog,[35] could affect Hes1 expression, and cross-talk between Hes family proteins and molecules in various cell signaling pathways, such as Stat3,[36] has been demonstrated.

We previously reported that Hes1 preserved highly purified hematopoietic stem cells in vitro and contributed to the expansion of transduced hematopoietic stem cells in the recipients' bone marrow,[7] but the effect of Hes1 transduction on myeloid progenitors was not evaluated in detail. We have now found the myeloid progenitor-immortalizing activity of Hes1. In addition, accumulation of KSL- and GMP-like population in Hes1-transduced cells implicates a role for Hes1 in leukemic stem cells. On the other hand, we have also found that the in vitro growth of the Hes1-immortalized cells is dependent on cytokine signaling and that Hes1 alone is insufficient to be fully leukemogenic when overexpressed. The mainstay of the Hes1 effects on myeloid progenitors appears to be blockade of differentiation, although other functions, such as reversion from the quiescent state to the actively cycling state,[21] may also be involved. In the present study, we confirmed that Hes1 expression represses C/EBP-α, a transcription factor having important roles in myeloid differentiation, in mouse KSLs and committed progenitors as we reported.[15] Moreover, transduction of C/EBP-α reversed the differentiation block caused by Hes1 expression, which partially explains the mechanism of blocked myeloid differentiation by Hes1. C/EBP-α is frequently mutated in AML with the normal karyotype.[37-39] In other human AML without C/EBP-α mutations, reduced C/EBP-α expression, possibly through deregulated epigenetic control, is not uncommon and is associated with poor prognosis.[40,41] Furthermore, mice injected with mutated C/EBP-α-transduced bone marrow cells develop myelodysplastic syndrome and AML.[42] Therefore, reduction of C/EBP-α function is highly relevant to the development and/or progression of myeloid malignancies. Hes1, therefore, might be involved in human myeloid malignancies through suppression of C/EBP-α.

Up-regulation of Hes1 is shown in a subset of human rhabdomyosarcomas[21] and medulloblastomas.[43,44] In the present study, we have detected elevated expression of Hes1 in 8 of the 20 samples from CML in blast crisis patients, but not those from CML

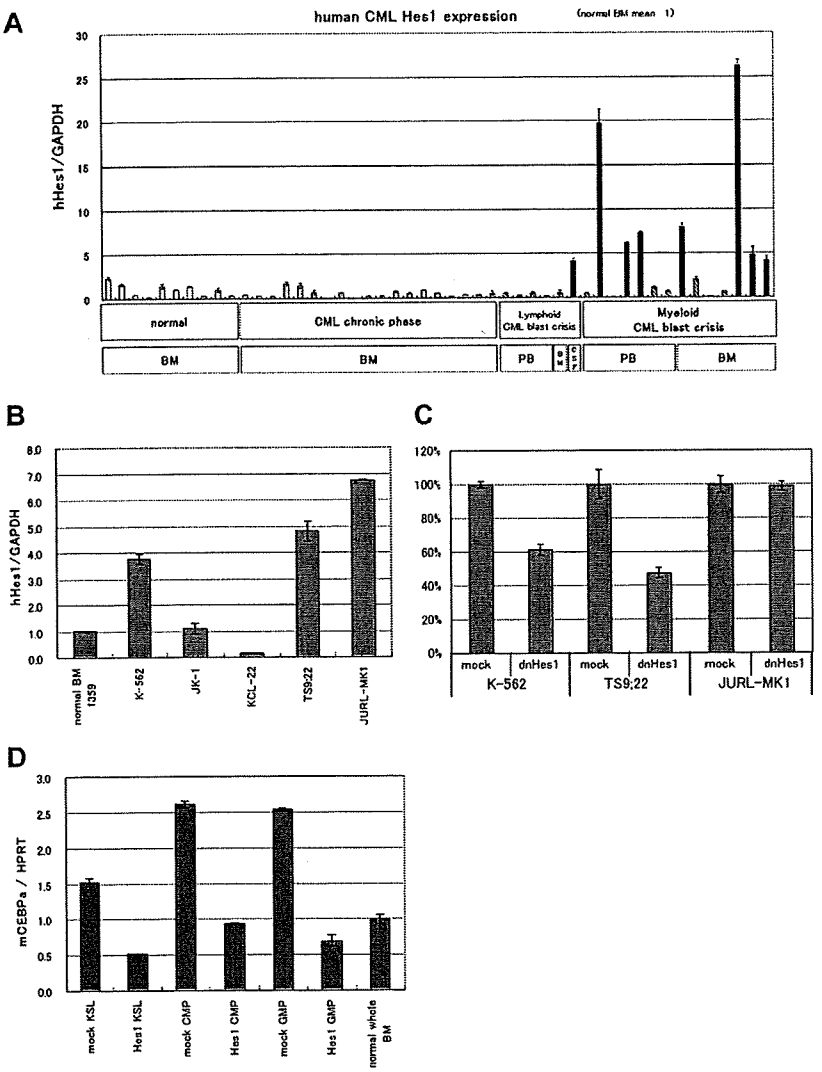

Figure 6. Hes1 expression was elevated in approximately 40% of patients with CML in blast crisis. (A) Real-time RT-PCR for Hes1 in bone marrow or peripheral blood cells from healthy subjects, patients with CML in chronic phase, or patients with CML in blast crisis. Expression levels were normalized by GAPDH mRNA. RNA from normal bone marrow cells served as a control (mean of 10 RNA levels of normal bone marrow was defined as 1). Hes1 mRNA levels exceeded 4 (solid bar) in 8 of 20 samples from CML in blast crisis patients. The correlation coefficient determined by the Wilcoxon signed-rank test between blast ratio and Hes1-expression level was −0.395. PB indicates peripheral blood; BM, bone marrow; CSF, cerebrospinal fluid. The solid bar represents CML in blast crisis exceeding 4; the hatched bar represents CML in blast crisis less than 4. (B) Hes1 expression in 5 human CML blast crisis cell lines. Expression levels of HES1 in K-562, JK-1, KCL-22, TS9:22, and JURL-MK1 were evaluated by real-time RT-PCR and were normalized by GAPDH mRNA. (C) Growth repression by transduction of dnHes1 (a dominant-negative Hes1) retrovirus vector into 3 human cell lines (K-562, TS9:22, and JURL-MK1). Six days after retrovirus transduction, cell numbers were counted. Growth is shown as a percentage of the control cells that were transduced with control vector. A representative result from 2 independent and reproducible experiments is shown. Error bars represent the SD from duplicate cultures. (D) Real-time RT-PCR for C/EBP-α in Hes1-transduced KSLs, CMPs, and GMPs compared with control vector-transduced KSLs, CMPs and GMPs. Total RNA was extracted at 60 hours from the initiation of Hes1-transduction. Error bars represent the SD from 2 independent experiments in (A-B,D).

in chronic phase patients. Although it is yet to be confirmed by a larger number of samples from CML as well as AML patients, this result indicates an interesting connection between the mouse model of AML/CML in blast crisis-like disease and human leukemia. In addition, we have demonstrated that transduction of dnHes1 represses the proliferation in 2 of 3 human cell lines of CML in blast crisis. These results suggest that Hes1 plays an important role in blast crisis of CML.

Although the origin of CML is considered to be a hematopoietic stem cell, blast crisis has been shown to be a result of transformation of myeloid progenitors.[16] BCR-ABL can cause MPN-like disease when introduced into the hematopoietic stem cell population but cannot induce MPN or leukemia when introduced into differentiated myeloid progenitors.[26] Therefore, development of full-blown AML/CML in blast crisis-like disease in mice with differentiated progenitors only by cotransduction with Hes1 and BCR-ABL may represent a true model of blast crisis of CML. In this context, Hes1 is a possible crisis-promoting gene like other examples, such as activated β-catenin[16] and BCL-2,[45] both of which caused CML in blast crisis-like disease in mice when transduced into GMPs together with BCR-ABL.

Several AML-associated fusion gene products, such as MLL-ENL,[46] MOZ-TIF2,[26] and MLL-AF9,[47] have been demonstrated to confer replating capacity on CMPs and GMPs, and eventually to transform these cells into leukemia-initiating cells. Unique to our findings is the fact that we transduced a wild-type transcription factor, Hes1, and found that such simple up-regulation of a transcription factor led to similar transformation phenotypes. A substantial number of examples have indicated that loss of function or altered function, rather than gain of function, of transcription factors, including MLL, MOZ, Runx1, RARα, C/EBP-α, etc, is associated with leukemogenesis. If up-regulation of Hes1 is indeed involved in human leukemias, this represents a new mechanism of leukemogenesis.

In modeling CML in mice, the present model provides a powerful tool by which we can induce 2 distinct phases of CML from stem cells or progenitors using BCR-ABL gene: a chronic phase-like state by transduction of KSL with BCR-ABL alone and a blast crisis-like state by cotransduction of CMPs and GMPs with BCR-ABL and Hes1.

In conclusion, we have developed a useful mouse model for CML blast crisis and have indicated that Hes1 is a key molecule in blast crisis transition in CML. The present mouse model will aid

Table 1. Clinical data of 20 patients with CML in blast crisis

Sample name	Source	Blast ratio	Hes1/GAPDH	Phenotype	Chromosome aberration	Clinical features
228 CML BC	PB	57	0.49	B-ALL	46,XY,t(9;22)/46,XY, +der(1;14)(q10;q12),t(9;22)	—
428 CML BC	PB	100	0.27	B-ALL	t(9;22)	—
984 CML BC	PB	60	0.56	B-ALL	46, XX, t(9;22)(q34;q11.2)	—
3259 CML BC	PB	100	0.16	B-ALL	t(9;22)	—
1385 CML BC	BM	81	0.56	B-ALL	t(9;22)	—
1107 CML BC	CSF	100	4.16	B-ALL	t(9;22)	The blasts increased drastically in CNS.
1 CML BC	PB	90	0.51	Myeloid	t(9;22)	—
219 CML BC	PB	12	19.72	Myeloid	45,XX,-7,t(9;22)	BM was dry tap composed of 100% blasts.
393 CML BC	PB	20	0.08	Myeloid	46,XX,t(9;22),add(17)(p11)	—
1088 CML BC	PB	30	6.22	Myeloid	46, XX, t(9;22)(q34;q11.2)	BM was dry tap.
1299 CML BC	PB	20	7.35	Myeloid	t(9;22)	BM was dry tap composed of 23% blasts.
1824 CML BC	PB	51	1.15	Myeloid	t(9;22)	BM was dry tap.
3153 CML BC	PB	7	0.66	Myeloid	t(9;22)	BM was dry tap. The blasts in BM increased up to 42% after taking this sample.
232 CML BC	BM	11	7.96	Myeloid	47,XY,+8,t(9;22)	The blasts in BM increased drastically up to 44% after taking this sample.
452 CML BC	BM	54	2.01	Myeloid	46,dic(17)(q10),t(9;22)	—
916 CML BC	BM	24	0.11	Myeloid	t(9;22)	—
1091 CML BC	BM	28	0.67	Myeloid	t(9;22)	—
811 CML BC	BM	25	26.25	Myeloid	46, XX, t(1;9;22)(q44;q34;q11.2)	—
3332 CML BC	BM	22	4.17	Myeloid	t(9;22)	—
3847 CML BC	BM	62	4.79	Myeloid	t(9;22)	—

CML indicates chronic myelogenous leukemia; BC, blast crisis; PB, peripheral blood; B-ALL, B-cell acute lymphoblastic leukemia; BM, bone marrow; CSF, cerebrospinal fluid; —, not applicable; and CNS, central nervous system.

understanding of the molecular mechanisms underlying blast crisis of CML and might lead to a better therapeutic outcome for this difficult disease.

Acknowledgments

The authors thank Dr R. Kageyama for the Hes1 cDNA; Dr H. Nakauchi and Dr M. Onodera for the GCDNsam/IRES-NGFR vector and the GCDNsam/IRES-GFP vector; Dr K. Akashi and Dr S. Mizuno for mouse C/EBP-α cDNA; Dr T. Inaba and Dr H. Asou (Hiroshima University, Hiroshima, Japan) for the JK-1, KCL-22, JURL-MK1 cell line; and Kirin Pharma for the TPO.

This work was supported by a Grant-in-Aid for Scientific Research (KAKENHI no. 20249051) and the Global Center of Excellence Program Center of Education and Research for the Advanced Genome-Based Medicine (for personalized medicine and the control of worldwide infectious diseases); the Ministry of Education, Culture, Sports, Science, and Technology of Japan (MEXT) and the Ministry of Health and Welfare of Japan (T.K.); and KAKENHI (no. 19390258), Astellas Foundation for Research on Metabolic Disorders, Uehara Memorial Foundation, and Princess Takamatsu Cancer Research Fund (S.C.).

Authorship

Contribution: F.N. did all the experiments and participated actively in writing the manuscript; M.S.-Y. and J.K. assisted with the experiments and actively participated in designing the experiments; Y.K., N.K., T.U., K.H., and K.K. assisted with the experiments; Y.H. and H.H. provided human samples; S.O. and M.K. participated in interpretation and designing the experiments; and T.K. and S.C. conceived the project, secured funding, and actively participated in manuscript writing.

Conflict-of-interest disclosure: T.K. serves as a consultant for R&D Systems and Rigel Pharmaceuticals. The remaining authors declare no competing financial interests.

Correspondence: Toshio Kitamura, Division of Stem Cell Signaling, Center for Stem Cell Therapy, Institute of Medical Science, University of Tokyo, 4-6-1 Shirokanedai, Minato-ku, Tokyo 108-8639, Japan; e-mail: kitamura@ims.u-tokyo.ac.jp; and Shigeru Chiba, Department of Hematology, Graduate School of Comprehensive Human Sciences, University of Tsukuba, 1-1-1 Tennodai, Tsukuba, Ibaraki 305-8575, Japan; e-mail: schiba-tky@umin.net.

References

1. Kageyama R, Nakanishi S. Helix-loop-helix factors in growth and differentiation of the vertebrate nervous system. *Curr Opin Genet Dev.* 1997;7(5):659-665.
2. Jarriault S, Brou C, Logeat F, Schroeter EH, Kopan R, Israel A. Signalling downstream of activated mammalian Notch. *Nature.* 1995;377(6547):355-358.
3. Jarriault S, Le Bail O, Hirsinger E, et al. Delta-1 activation of notch-1 signaling results in HES-1 transactivation. *Mol Cell Biol.* 1998;18(12):7423-7431.
4. Johnson JE, Birren SJ, Anderson DJ. Two rat homologues of Drosophila achaete-scute specifically expressed in neuronal precursors. *Nature.* 1990;346(6287):858-861.
5. Sumazaki R, Shiojiri N, Isoyama S, et al. Conversion of biliary system to pancreatic tissue in Hes1-deficient mice. *Nat Genet.* 2004;36(1):83-87.
6. Kumano K, Chiba S, Shimizu K, et al. Notch1 inhibits differentiation of hematopoietic cells by sustaining GATA-2 expression. *Blood.* 2001;98(12):3283-3289.
7. Kunisato A, Chiba S, Nakagami-Yamaguchi E, et al. HES-1 preserves purified hematopoietic stem cells ex vivo and accumulates side population cells in vivo. *Blood.* 2003;101(5):1777-1783.
8. Kaneta M, Osawa M, Sudo K, Nakauchi H, Farr AG, Takahama Y. A role for pref-1 and HES-1 in thymocyte development. *J Immunol.* 2000;164(1):256-264.
9. Tomita K, Hattori M, Nakamura E, Nakanishi S, Minato N, Kageyama R. The bHLH gene Hes1 is essential for expansion of early T cell precursors. *Genes Dev.* 1999;13(9):1203-1210.
10. Weng AP, Ferrando AA, Lee W, et al. Activating mutations of NOTCH1 in human T cell acute lymphoblastic leukemia. *Science.* 2004;306(5694):269-271.
11. Lee S-y, Kumano K, Nakazaki K, et al. Gain-of-function mutations and copy number increases of

Notch2 in diffuse large B-cell lymphoma. *Cancer Sci.* 2009;100(5):920-926.

12. Radtke F, Wilson A, Mancini SJ, MacDonald HR. Notch regulation of lymphocyte development and function. *Nat Immunol.* 2004;5(3):247-253.
13. Allman D, Punt JA, Izon DJ, Aster JC, Pear WS. An invitation to T and more: notch signaling in lymphopoiesis. *Cell.* 2002;109[suppl]:S1-S11.
14. Radtke F, Wilson A, Stark G, et al. Deficient T cell fate specification in mice with an induced inactivation of Notch1. *Immunity.* 1999;10(5):547-558.
15. Sakata-Yanagimoto M, Nakagami-Yamaguchi E, Saito T, et al. Coordinated regulation of transcription factors through Notch2 is an important mediator of mast cell fate. *Proc Natl Acad Sci U S A.* 2008;105(22):7839-7844.
16. Jamieson CH, Ailles LE, Dylla SJ, et al. Granulocyte-macrophage progenitors as candidate leukemic stem cells in blast-crisis CML. *N Engl J Med.* 2004; 351(7):657-667.
17. Akashi K, Traver D, Miyamoto T, Weissman IL. A clonogenic common myeloid progenitor that gives rise to all myeloid lineages. *Nature.* 2000; 404(6774):193-197.
18. Honda H, Fujii T, Takatoku M, et al. Expression of p210bcr/abl by metallothionein promoter induced T-cell leukemia in transgenic mice. *Blood.* 1995; 85(10):2853-2861.
19. Kitamura T, Koshino Y, Shibata F, et al. Retrovirus-mediated gene transfer and expression cloning: powerful tools in functional genomics. *Exp Hematol.* 2003;31(11):1007-1014.
20. Morita S, Kojima T, Kitamura T. Plat-E: an efficient and stable system for transient packaging of retroviruses. *Gene Ther.* 2000;7(12):1063-1066.
21. Sang L, Coller HA, Roberts JM. Control of the reversibility of cellular quiescence by the transcriptional repressor HES1. *Science.* 2008; 321(5892):1095-1100.
22. Hopfer O, Zwahlen D, Fey MF, Aebi S. The Notch pathway in ovarian carcinomas and adenomas. *Br J Cancer.* 2005;93(6):709-718.
23. Iwasaki H, Mizuno S, Mayfield R, et al. Identification of eosinophil lineage-committed progenitors in the murine bone marrow. *J Exp Med.* 2005; 201(12):1891-1897.
24. Ono R, Nakajima H, Ozaki K, et al. Dimerization of MLL fusion proteins and FLT3 activation synergize to induce multiple-lineage leukemogenesis. *J Clin Invest.* 2005;115(4):919-929.
25. Kawamata S, Du C, Li K, Lavau C. Overexpression of the Notch target genes Hes in vivo induces lymphoid and myeloid alterations. *Oncogene.* 2002;21(24):3855-3863.
26. Huntly BJ, Shigematsu H, Deguchi K, et al. MOZ-TIF2, but not BCR-ABL, confers properties of leukemic stem cells to committed murine hematopoietic progenitors. *Cancer Cell.* 2004;6(6):587-596.
27. Lozzio CB, Lozzio BB. Human chronic myelogenous leukemia cell-line with positive Philadelphia chromosome. *Blood.* 1975;45(3):321-334.
28. Okuno Y, Suzuki A, Ichiba S, et al. Establishment of an erythroid cell line (JK-1) that spontaneously differentiates to red cells. *Cancer.* 1990;66(7): 1544-1551.
29. Kubonishi I, Miyoshi I. Establishment of a Ph1 chromosome-positive cell line from chronic myelogenous leukemia in blast crisis. *Int J Cell Cloning.* 1983;1(2):105-117.
30. Gotoh A, Miyazawa K, Ohyashiki K, et al. Tyrosine phosphorylation and activation of focal adhesion kinase (p125FAK) by BCR-ABL oncoprotein. *Exp Hematol.* 1995;23(11):1153-1159.
31. Di Noto R, Luciano L, Lo Pardo C, et al. JURL-MK1 (c-kit(high)/CD30-/CD40-) and JURL-MK2 (c-kit(low)/CD30+/CD40+) cell lines: 'two-sided' model for investigating leukemic megakaryocytopoiesis. *Leukemia.* 1997;11(9):1554-1564.
32. Lee SY, Kumano K, Masuda S, et al. Mutations of the Notch1 gene in T-cell acute lymphoblastic leukemia: analysis in adults and children. *Leukemia.* 2005;19(10):1841-1843.
33. Allenspach EJ, Maillard I, Aster JC, Pear WS. Notch signaling in cancer. *Cancer Biol Ther.* 2002;1(5):466-476.
34. Fu L, Kogoshi H, Nara N, Tohda S. NOTCH1 mutations are rare in acute myeloid leukemia. *Leuk Lymphoma.* 2006;47(11):2400-2403.
35. Ingram WJ, McCue KI, Tran TH, Hallahan AR, Wainwright BJ. Sonic Hedgehog regulates Hes1 through a novel mechanism that is independent of canonical Notch pathway signalling. *Oncogene.* 2008;27(10):1489-1500.
36. Kamakura S, Oishi K, Yoshimatsu T, Nakafuku M, Masuyama N, Gotoh Y. Hes binding to STAT3 mediates crosstalk between Notch and JAK-STAT signalling. *Nat Cell Biol.* 2004;6(6):547-554.
37. Nerlov C. C/EBPalpha mutations in acute myeloid leukaemias. *Nat Rev Cancer.* 2004;4(5):394-400.
38. Gombart AF, Hofmann WK, Kawano S, et al. Mutations in the gene encoding the transcription factor CCAAT/enhancer binding protein alpha in myelodysplastic syndromes and acute myeloid leukemias. *Blood.* 2002;99(4):1332-1340.
39. Smith ML, Cavenagh JD, Lister TA, Fitzgibbon J. Mutation of CEBPA in familial acute myeloid leukemia. *N Engl J Med.* 2004;351(23):2403-2407.
40. Zhang P, Iwasaki-Arai J, Iwasaki H, et al. Enhancement of hematopoietic stem cell repopulating capacity and self-renewal in the absence of the transcription factor C/EBP alpha. *Immunity.* 2004;21(6):853-863.
41. Koschmieder S, Halmos B, Levantini E, Tenen DG. Dysregulation of the C/EBPalpha differentiation pathway in human cancer. *J Clin Oncol.* 2009;27(4):619-628.
42. Kirstetter P, Schuster MB, Bereshchenko O, et al. Modeling of C/EBPalpha mutant acute myeloid leukemia reveals a common expression signature of committed myeloid leukemia-initiating cells. *Cancer Cell.* 2008;13(4):299-310.
43. Fan X, Mikolaenko I, Elhassan I, et al. Notch1 and notch2 have opposite effects on embryonal brain tumor growth. *Cancer Res.* 2004;64(21): 7787-7793.
44. Hallahan AR, Pritchard JI, Hansen S, et al. The SmoA1 mouse model reveals that notch signaling is critical for the growth and survival of sonic hedgehog-induced medulloblastomas. *Cancer Res.* 2004;64(21):7794-7800.
45. Jaiswal S, Traver D, Miyamoto T, Akashi K, Lagasse E, Weissman IL. Expression of BCR/ABL and BCL-2 in myeloid progenitors leads to myeloid leukemias. *Proc Natl Acad Sci U S A.* 2003;100(17):10002-10007.
46. Cozzio A, Passegue E, Ayton PM, Karsunky H, Cleary ML, Weissman IL. Similar MLL-associated leukemias arising from self-renewing stem cells and short-lived myeloid progenitors. *Genes Dev.* 2003;17(24):3029-3035.
47. Krivtsov AV, Twomey D, Feng Z, et al. Transformation from committed progenitor to leukaemia stem cell initiated by MLL-AF9. *Nature.* 2006;442(7104): 818-822.

MOLECULAR AND CELLULAR BIOLOGY, Apr. 2009, p. 1796–1813
0270-7306/09/$08.00+0 doi:10.1128/MCB.01423-08

Vol. 29, No. 7

A Rac GTPase-Activating Protein, MgcRacGAP, Is a Nuclear Localizing Signal-Containing Nuclear Chaperone in the Activation of STAT Transcription Factors▽†

Toshiyuki Kawashima,[1]‡* Ying Chun Bao,[1]‡ Yukinori Minoshima,[1] Yasushi Nomura,[1] Tomonori Hatori,[1] Tetsuya Hori,[2] Tatsuo Fukagawa,[2] Toshiyuki Fukada,[3,4] Noriko Takahashi,[1] Tetsuya Nosaka,[1,5] Makoto Inoue,[6] Tomohiro Sato,[6,7] Mutsuko Kukimoto-Niino,[6] Mikako Shirouzu,[6] Shigeyuki Yokoyama,[6,7] and Toshio Kitamura[1]*

Division of Cellular Therapy, Institute of Medical Science, University of Tokyo, Minato-ku, Tokyo 108-8639, Japan[1]; Department of Molecular Genetics, National Institute of Genetics and the Graduate University for Advanced Studies, Mishima, Shizuoka 411-8540, Japan[2]; Laboratory for Cytokine Signaling, RIKEN Research Center for Allergy and Immunology,[3] and Protein Research Group, Genomic Sciences Center, Yokohama Institute, RIKEN,[6] 1-7-22 Suehiro-cho, Tsurumi, Yokohama 230-0045, Japan; Department of Allergy and Immunology, Osaka University Graduate School of Medicine, Osaka University, 2-2 Yamada-oka, Suita, Osaka 565-0871, Japan[4]; Department of Microbiology, Mie University Graduate School of Medicine, 2-174 Edobashi, Tsu 514-8507, Japan[5]; and Department of Biophysics and Biochemistry, Graduate School of Science, University of Tokyo, 7-3-1 Hongo, Bunkyo-ku, Tokyo 113-0033, Japan[7]

Received 10 September 2008/Returned for modification 1 November 2008/Accepted 12 January 2009

In addition to their pleiotropic functions under physiological conditions, transcription factors STAT3 and STAT5 also have oncogenic activities, but how activated STATs are transported to the nucleus has not been fully understood. Here we show that an MgcRacGAP mutant lacking its nuclear localizing signal (NLS) blocks nuclear translocation of p-STATs both in vitro and in vivo. Unlike wild-type MgcRacGAP, this mutant did not promote complex formation of phosphorylated STATs (p-STATs) with importin α in the presence of GTP-bound Rac1, suggesting that MgcRacGAP functions as an NLS-containing nuclear chaperone. We also demonstrate that mutants of STATs lacking the MgcRacGAP binding site (the strand βb) are hardly tyrosine phosphorylated after cytokine stimulation. Intriguingly, mutants harboring small deletions in the C′-adjacent region (βb-βc loop region) of the strand βb became constitutively active with the enhanced binding to MgcRacGAP. The molecular basis of this phenomenon will be discussed, based on the computer-assisted tertiary structure models of STAT3. Thus, MgcRacGAP functions as both a critical mediator of STAT's tyrosine phosphorylation and an NLS-containing nuclear chaperone of p-STATs.

The STAT (signal transducers and activators of transcription) family proteins (STAT1 to -4, -5A, -5B, and -6) are phosphorylated by cytokine stimulation, form homo- or heterodimers, and enter the nucleus, where they regulate expression of their target genes (6, 13). STATs have a variety of functions, including antiapoptosis, proliferation, differentiation, inflammation, and development under physiological conditions, and of note, the oncogenic activities of STAT3 and STAT5 have also been demonstrated under pathological conditions (5).

A small GTPase Rac1 is implicated in cytoskeletal organization, membrane ruffling, production of superoxide, phagocytosis, and chemotaxis as well as regulation of the cell cycle (15, 39). Recent studies revealed its distinct roles in nuclear translocation of phosphorylated STATs (p-STATs) and β-catenin and also its nuclear accumulation in the G_2 phase, promoting cell division (17, 31, 47). MgcRacGAP is an evolutionarily conserved GTPase-activating protein (GAP) for Rho family GTPases. We and others previously showed that MgcRacGAP controls the mitotic spindle through associating α-, β-, and γ-tubulin, Rho family GTPases, and a kinesin protein, MKLP1, and plays essential roles in the completion of cytokinesis, accumulating to the midbody (12, 16, 32). Very recently, Yamada et al. reported that conditional knockout of MgcRacGAP results in acute apoptosis even before the failure of cytokinesis in interleukin-7 (IL-7)-expanded $B220^+$ cells (48), indicating that MgcRacGAP is not simply involved in cell division but also in cell survival, at least in IL-7-expanded $B220^+$ cells.

Molecular trafficking between the nucleus and cytoplasm occurs via nuclear pore complexes. To enter the nucleus, nuclear proteins larger than ~50 kDa usually harbor a functional nuclear localization signal (NLS) or bind NLS-containing chaperones. The best-characterized NLS is the mono- or bipartite polybasic NLS. Polybasic NLS-containing proteins are usually recognized by importin α/β heterodimers, importin β docks the ternary complex to the nuclear pore, and the complex migrates into the nucleus. Then, the GTP-bound form of small GTPase Ran directly binds to importin β in the complex,

* Corresponding author. Mailing address: Division of Cellular Therapy, Institute of Medical Science, University of Tokyo, Minato-ku, Tokyo 108-8639, Japan. Phone: 81-3-5449-5758. Fax: 81-3-5449-5453. E-mail for Toshiyuki Kawashima: kkawa@ims.u-tokyo.ac.jp. E-mail for Toshio Kitamura: kitamura@ims.u-tokyo.ac.jp.

† Supplemental material for this article may be found at http://mcb.asm.org/.

‡ T.K. and Y.C.B. contributed equally to this work.

▽ Published ahead of print on 21 January 2009.

followed by disassembly of the complex inside the nucleus (11, 29). In addition to the polybasic NLS proline, tyrosine-containing NLSs (PY-NLSs) have been reported to be a different class of NLS; these NLSs mediate direct binding of NLS-containing proteins to karyopherin β2 (24).

How activated STATs are transported to the nucleus has been investigated; activated STAT1 and STAT3 were reported to bind importin α5 and several importin αs, respectively, which mediated the nuclear transport of STATs (25, 26, 30, 42, 44). Molecules other than importins and Ran also participate in the regulation of the nuclear translocation of STATs (27). We recently found that GTP-bound Rac1 and MgcRacGAP form a ternary complex with p-STATs and play critical roles in the nuclear translocation of p-STATs via the importin α/β pathway in an in vitro nuclear transport assay (17). However, it remained elusive how GTP-bound Rac1 and MgcRacGAP mediate the complex formation of p-STATs with importin αs. Moreover, the regulation of nuclear import of activated STATs by MgcRacGAP has not been fully demonstrated in vivo, because MgcRacGAP also plays an essential role in the completion of cytokinesis (12, 16, 33, 45). Therefore, the phenotypes observed in MgcRacGAP-depleted cells may include the effects of cytokinesis failure.

In the present work, we demonstrate that the NLS of MgcRacGAP plays essential roles in the nuclear import of p-STATs not only in vitro but also in vivo, by using MgcRacGAP conditional knockout DT40 cells expressing MgcRacGAP mutants lacking the NLS. We also found that the STAT mutants that did not bind MgcRacGAP were hardly phosphorylated on their tyrosine residues by cytokine stimulation, while the STAT mutants that preferentially bound MgcRacGAP exerted strong transcriptional activities even without cytokine stimulation. Thus, MgcRacGAP accompanied by GTP-bound Rac1 is not only an NLS-containing nuclear chaperone of p-STATs but also a critical activator of STAT proteins.

MATERIALS AND METHODS

Purification of recombinant proteins in Sf-9 cells. Purification of recombinant proteins using Sf-9 cells was done as described previously (17). To confirm the purity, the eluted proteins were subjected to sodium dodecyl sulfate-polyacrylamide gel electrophoresis (SDS-PAGE), followed by Coomassie blue (CBB) staining or by Western blotting. Purified His-tagged L69Ran and His-tagged N24Ran were purchased from Cytoskeleton, Inc.

Import assays with permeabilized cells. HeLa cells were grown on poly(L-lysine)-coated coverslips and permeabilized with 40 μg/ml digitonin (Roche) in transport buffer (TB; 20 mM HEPES, pH 7.3, 110 mM KO-acetate, 2 mM $Mg(O\text{-acetate})_2$, 1 mM EGTA, 2 mM dithiothreitol, 0.4 mM phenylmethylsulfonyl fluoride, 3 μg/ml of aprotinin, 2 μg/ml of pepstatin A, 1 μg/ml of leupeptin, 20 mg/ml of bovine serum albumin) for 10 min at room temperature. Subsequently, the cells were washed twice in TB to wash out cytoplasmic proteins. Incubation with 50 μl import mix (IM) was performed at 37°C for 30 min. The IM contained TB, an energy-regenerating system (ERS; 0.5 mM ATP, 0.5 mM GTP, 10 mM creatine phosphate, 30 U/ml creatine phosphokinase) and combinations of 1 μM of the purified proteins indicated in Fig. 2B, below (see also Fig. S2 and S3 in the supplemental material). Following the import reaction, the cells were washed with ice-cold TB and immunostained.

Immunostaining and antibodies. HeLa cells were immunostained as described previously (12). Rabbit anti-STAT5A, anti-STAT3, antihemagglutinin, anti-NF-κB p65, goat anti-glutathione *S*-transferase (anti-GST) (Santa Cruz), mouse anti-Flag (M2; Sigma), rabbit anti-Flag (Zymed), and affinity-purified rabbit anti-MgcRasGAP (12) antibodies (Abs) were used for the first Ab. For the secondary Ab and DNA staining, fluorescein isothiocyanate- or rhodamine-conjugated goat anti-rabbit immunoglobulin (Ig; Wako), fluorescein isothiocyanate- or rhodamine-conjugated goat anti-mouse Ig (Sigma), or rhodamine-conjugated anti-goat Ig (Wako) and 4′,6-diamino-2-phenylindole (DAPI) were used.

Microscopy. Fixed fluorescence images were analyzed on a confocal microscope (FLUOVIEW FV300 scanning laser biological microscope IX70 system; Olympus). Living cells expressing green fluorescent protein (GFP)-fusion proteins were viewed with a fluorescence microscope IX70 (Olympus) equipped with a SenSys/OL cold charge-coupled-device camera (Olympus).

In vitro binding assay, immunoprecipitation, and Western blotting. Immunoprecipitation, gel electrophoresis, and immunoblotting were done as described previously (17), with minor modifications. Purified proteins which were preincubated in the TB with 0.5% Triton X in the in vitro binding assay or cell lysates (2×10^7 cells/ml) were incubated at 4°C for 2 h with the indicated antibodies and protein A-Sepharose. The immunoprecipitates were subjected to Western blot analysis with an anti-tyrosine-phosphorylated STAT5 monoclonal Ab (anti-p-STAT5; Upstate), anti-MgcRacGAP (12), anti-importin β1 (Transduction Laboratories), or anti-MKLP-1, anti-STAT5A, anti-Rac1, or anti-importin α1 (Santa Cruz) antibodies. The filter-bound Ab were detected using the enhanced chemiluminescence system (Amersham). Cytosol and nuclear fractions were prepared, as described previously (17). Fractionation was confirmed by Western blotting with the anti-histone deacetylase (HDAC; for the nuclear fraction) or RhoA (for the cytosol fraction) Ab (Santa Cruz).

Generation of MgcRacGAP conditional knockout cells (5C cells) using DT40 cells. Full-length MgcRacGAP cDNA was cloned into the EcoRI/BamHI site of pUHD10-3 to yield a tetracycline (TET)-sensitive expression plasmid, pUHD-MgcRacGAP. For targeting constructs, a histidinol (hisD) or puromycin (puro) resistance cassette under the control of the β-actin promoter was inserted between the two arms. The targeting constructs and pUHD-MgcRacGAP were transfected into DT40 cells with a GenePulser II electroporator (Bio-Rad). DT40 cells were cultured and transfected as described previously (32). All DT40 cells were cultured at 38°C in Dulbecco's modified medium supplemented with 10% fetal calf serum, 1% chicken serum, penicillin, and streptomycin. To suppress expression of the tetracycline-responsive transgenes, TET (Sigma) was added to the culture medium at a final concentration of 2 μg/ml.

Expression constructs. Flag-tagged wild-type (WT) and mutant MgcRacGAP or STATs were cloned into EcoRI and NotI sites of a mammalian expression vector, pME 18S, or a retrovirus expression vector, pMXs-IG and pMXs-neo. The deletion constructs of MgcRacGAP that lack the internal (INT) domain or various regions of the INT domain were generated by overlapping extension using PCR as described in reference 18. Synthesized oligonucleotides encoding the NLS of MgcRacGAP (NLS-MgcRacGAP; amino acids [aa] 182 to 200), mutant NLS of MgcRacGAP (NLS-MgcRacGAP-182AAA/199AA), or the large T antigen-NLS (PKKKRKV) were cloned into EcoRI and NotI sites of a pMXs-GFP-fusion vector. Site-directed mutagenesis of MgcRacGAP or STATs was done using QuikChange (Stratagene) and the oligonucleotide primers. Several alanine substitution mutants were generated by overlapping extension using PCR. The sequence generated by PCR was confirmed by automated sequencing using an ABI Prism 310 genetic analyzer (Perkin-Elmer).

Production of retroviruses. High-titer retroviruses harboring Cre-recombinase were produced in transient retrovirus packaging cell line PLAT-E or PLAT-A (36).

Cell culture and transfection. The 293T cells were grown in Dulbecco's modified Eagle medium supplemented with 5% fetal calf serum and were transiently transfected with plasmids encoding the wild-type or the mutant forms of STATs using Lipofectamine Plus (Gibco-BRL) according to the manufacturer's recommendations.

Luciferase reporter assay. For the experiments using DT40 cells, pMKIT (mock) or pMKIT/ITD-Flt3 together with 1.0 μg of pME/STAT5A, 1.0 μg of a reporter plasmid carrying a firefly luciferase gene driven by the β-casein promoter, and 0.5 μg of an internal control reporter plasmid with the Rous sarcoma virus long terminal repeat promoter was introduced into 2×10^6 cells of 5C cells with Nucleofector II (Amaxa) set at program B-009 using the Cell Line Nucleofector kit T (Amaxa) according to the manufacturer's instruction. A control vector carrying GFP was introduced to more than 50% of 5C cells under this condition. Sixteen hours after transfection, cells were lysed and were then subjected to a dual luciferase reporter system (Promega). Luciferase activities were also examined in the lysates of 5C transfectants cotransfected with the NF-κB reporter plasmid (k9) carrying a firefly luciferase gene driven by the IL-6 promoter (14) together with an internal control plasmid. After the transfection, cells were incubated with 30 nM phorbol myristate acetate (PMA) and 1 μM ionomycin for 12 h before cell lysates were prepared. For the experiments using 293T cells, cells were transfected with pME (mock) or pME/STAT5As together with 0.5 μg of pME/EPOR, 0.5 μg of a reporter plasmid carrying a firefly luciferase gene driven by the β-casein promoter, and 0.5 μg of an internal control reporter

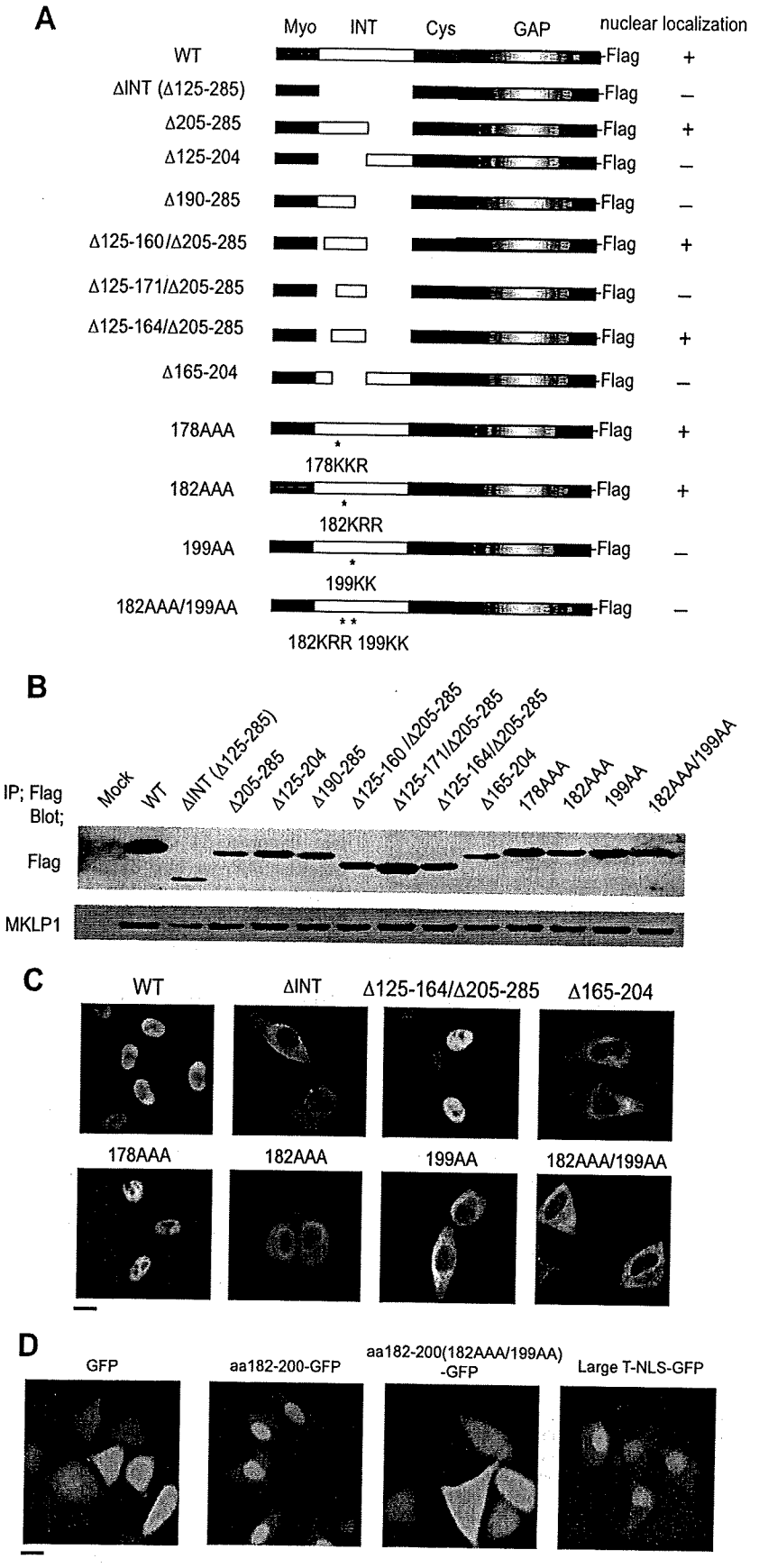
A
Myo
INT
Cys
GAP
nuclear localization
WT
Flag
+
ΔINT (Δ125-285)
Flag
–
Δ205-285
Flag
+
Δ125-204
Flag
–
Δ190-285
Flag
–
Δ125-160/Δ205-285
Flag
+
Δ125-171/Δ205-285
Flag
–
Δ125-164/Δ205-285
Flag
+
Δ165-204
Flag
–
178AAA
Flag
+
178KKR
182AAA
Flag
+
182KRR
199AA
Flag
–
199KK
182AAA/199AA
Flag
–
182KRR 199KK
B
IP; Flag
Blot;
Mock
WT
ΔINT (Δ125-285)
Δ205-285
Δ125-204
Δ190-285
Δ125-160 /Δ205-285
Δ125-171/Δ205-285
Δ125-164/Δ205-285
Δ165-204
178AAA
182AAA
199AA
182AAA/199AA
Flag
MKLP1
C
WT
ΔINT
Δ125-164/Δ205-285
Δ165-204
178AAA
182AAA
199AA
182AAA/199AA
D
GFP
aa182-200-GFP
aa182-200(182AAA/199AA)
-GFP
Large T-NLS-GFP

plasmid with the Rous sarcoma virus long terminal repeat promoter, using Lipofectamine Plus (Gibco-BRL). Twenty-four hours after transfection, cells were stimulated with erythropoietin (EPO; 18 ng/ml; 16 h) and subjected to a dual luciferase reporter system (Promega). To examine the transcriptional activities of STAT3 mutants harboring deletions in DB2, a luciferase assay was done in the lysates of unstimulated or IL-6-stimulated (20 ng/ml) and sIL-6R-stimulated (20 ng/ml) 293T cells cotransfected with the STAT3 reporter plasmid carrying a firefly luciferase gene driven by the mouse glial fibrillary acidic protein promoter (35) together with an internal control reporter plasmid and either the mock vector (pME), the expression vector for the Flag-tagged WT STAT3, or a series of STAT3 mutants harboring deletions in DB2.

Semiquantitative RT-PCR. Gene expression was examined by semiquantitative reverse transcription-PCR (RT-PCR) analysis. One microgram of total RNA was reverse transcribed with random hexamers by using a first-strand cDNA synthesis kit (Pharmacia), and the reaction mixture was subjected to PCR. PCRs were carried out using the following oligonucleotide primers: chicken *Bcl-xL* sense (5′-CGTACCAGAGCTTTGAGCAGGT-3′) and antisense (5′-GACCA AGCACAAGCACAATCAC-3′) and chicken glyceraldehyde-3-phosphate dehydrogenase (*GAPDH*) sense (5′-ATGGTGAAAGTCGGAGTCAACGG-3′) and antisense (5′-ACAGTGCCCTTGAAGTGTCC-3′). PCR was performed under the following conditions to amplify the chicken *Bcl-xL* gene: 96°C for 3 min; 30 cycles of 96°C for 30 s, 63°C for 30 s, and 72°C for 30 s; a final elongation at 72°C for 8 min. To amplify the *GAPDH* gene, conditions were 96°C for 3 min, 20 cycles of 96°C for 30 s, 55°C for 30 s, and 72°C for 30 s, and a final elongation at 72°C for 8 min. Amplification of the product is not saturated at this number of cycles.

Modeling of mutant structures. The models of the D1-10, d356P, d357E, d358L, and L358A mutants of STAT3 were built using the 2.25-Å resolution crystal structure of the STAT3β · DNA complex (2) (PDB ID 1BG1) as a template. Initial models were constructed with the MODELER 9v1 program (9, 28, 41). Then, the models were refined by energy minimization with the AMBER99 force field (46) using MOE computer software (Chemical Computing Group Inc.).

RESULTS

The INT domain of MgcRacGAP contains the bipartite NLS. While endogenous MgcRacGAP localizes both in the cytoplasm and nucleus, overexpressed exogeneous MgcRacGAP mainly accumulates to the nucleus in the interphase in HeLa cells (12). Although MgcRacGAP does not harbor a classic (polybasic) NLS, we found that the ΔINT mutant localized in the cytoplasm (Fig. 1C). These results suggested that the INT domain was critical for the nuclear translocation of MgcRacGAP. To identify a functional NLS of MgcRacGAP, we produced a series of Flag-tagged deletion mutants of the INT domain (Fig. 1A). Protein expression of the mutants and their interaction with a known binding partner, MKLP-1 (34), were confirmed by immunoprecipitation and Western blotting using anti-Flag Ab and anti-MKLP-1 Ab (Fig. 1B). After the immunostaining experiments in HeLa cells, we found that aa 165 to 204 of MgcRacGAP were required for its nuclear localization (Fig. 1C). Since this region contained three polybasic regions (178KKR, 182KRR, and 199KK), we tested whether these polybasic regions could serve as an NLS. We produced alanine substitution mutants (178AAA, 182AAA, 199AA, and 182AAA/199AA) and tested their subcellular localizations. While the 178AAA mutant was located in the nucleus, the 182AAA mutant showed partial cytoplasmic localization, and the 199AA and 182AAA/199AA mutants mostly localized in cytoplasm (Fig. 1C). Next, aa182-200, aa182-200(182AAA/199AA), and a conventional NLS of large T antigen were fused to the N terminus of GFP and we viewed their subcellular localizations with a fluorescence microscope in living cells. As shown in Fig. 1D, aa182-200–GFP and large T-NLS-GFP but not GFP alone or aa182-200(182AAA/199AA)–GFP preferentially accumulated to the nucleus, indicating that aa 182 to 200 is sufficient for a functional polybasic NLS. We also confirmed that leptomycin B treatment, which inhibits nuclear export signal-dependent nuclear export by specific binding to CRM1, did not affect the nuclear or cytoplasmic localization of the WT or 182AAA/199AA mutant, respectively (data not shown). These results suggest that 182KRR and 199KK serve as a functional bipartite NLS for MgcRacGAP. Next, we asked whether MgcRacGAP was transported into the nucleus by importin family members like other proteins carrying NLS. β1Δ450-876, a mutant of importin β1 which lacks the importin α binding site, thereby competitively blocking importin α/β-mediated nuclear import (21), strongly inhibited the nuclear translocation of MgcRacGAP (data not shown). These results implied that MgcRacGAP was transported to the nucleus in an importin α/β-dependent manner.

Importin αs specifically bind MgcRacGAP in yeast through its bipartite NLS. To determine which member of the importin α family is involved in the nuclear transport of MgcRacGAP, we used a yeast two-hybrid system. To test another possibility, that importin β1 directly mediates the nuclear import of MgcRacGAP, we also examined whether importin β1 could directly bind MgcRacGAP. It was found that importin αs specifically bound MgcRacGAP in yeast (see Fig. S1A in the supplemental material). Moreover, purified importin α1 but not importin β1 pulled down MgcRacGAP from HeLa cell lysate (see Fig. S1B in the supplemental material), suggesting that importin α1 but not importin β1 directly bound MgcRacGAP. The purity of isolated importin α1 and importin β1 was confirmed by CBB staining (see Fig. S1C in the supplemental material). To determine if the bipartite NLS of MgcRacGAP indeed mediated its association with importin α1, we tested the interaction of importin α1 with the INT domain, aa 165 to 205, or each of the alanine mutants of MgcRacGAP (182AAA, 199AA, and 182AAA/199AA), and confirmed that the interaction between importin α1 and MgcRacGAP was mediated by the bipartite NLS of MgcRacGAP (see Fig. S1D in the supplemental material). These results demonstrated that MgcRac-

FIG. 1. Identification of the nuclear localization signal of MgcRacGAP. (A) Schematic diagram of various Flag-tagged deletion mutants in the INT domain of MgcRacGAP and summary of the localizations of these mutants. (B) Expression of various deletion mutants and their potential to interact with a known partner, MKLP-1. Cells were transfected with expression vectors carrying Flag-tagged WT or various deletion mutants in the INT domain. After 36 h, cells were immunoprecipitated with the anti-Flag Ab and blotted with the anti-Flag Ab (upper panel) or anti-MKLP-1 Ab (lower panel). (C) Localization of Flag-tagged WT and various deletion mutants in the INT domain of MgcRacGAP in HeLa cells. Cells were transfected with expression vectors carrying Flag-tagged WT or various deletion mutants in the INT domain. After 36 h, cells were immunostained with the anti-Flag Ab (green) and DAPI (blue) and viewed with a fluorescence microscope IX70 (Olympus). Bar, 10 μm. (D) Localization of GFP-fused NLS of MgcRacGAP. GFP-fused aa182-200 of MgcRacGAP, aa182-200(182AAA/199AA), and large T antigen-NLS were expressed in HeLa cells. After 36 h, living cells were viewed with a fluorescence IX70 microscope (Olympus). Bar, 10 μm.

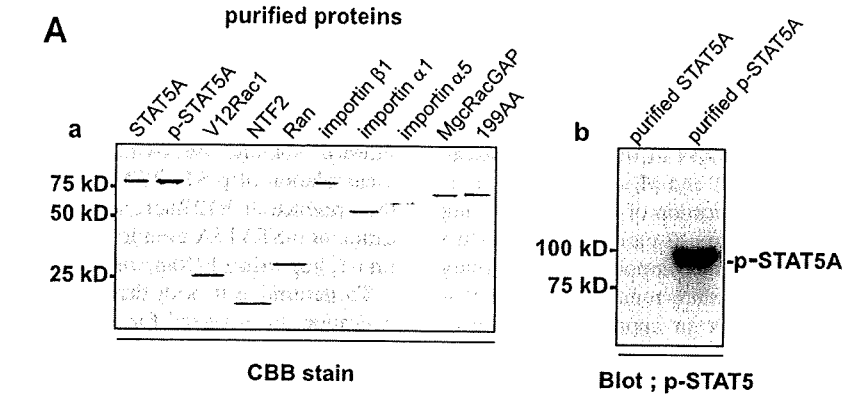
A
purified proteins
a
STAT5A
p-STAT5A
V12Rac1
NTF2
Ran
importin β1
importin α1
importin α5
MgcRacGAP
199AA
75 kD
50 kD
25 kD
CBB stain
b
purified STAT5A
purified p-STAT5A
100 kD
75 kD
-p-STAT5A
Blot ; p-STAT5

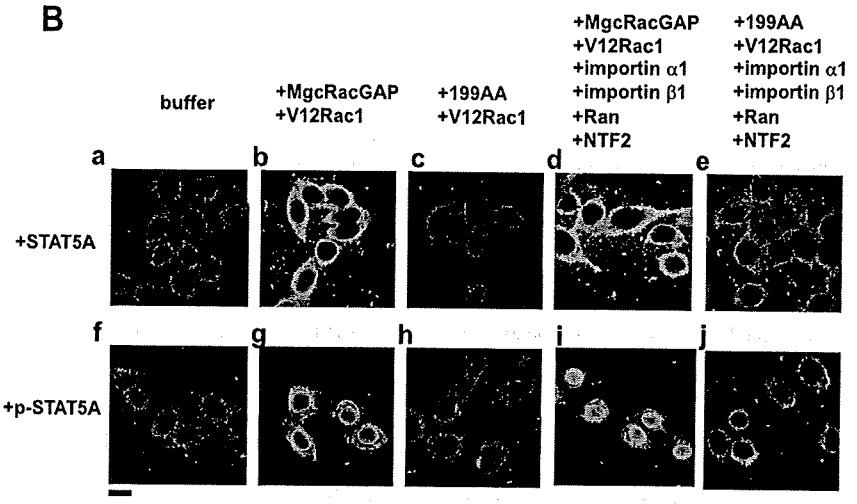
B
buffer
+MgcRacGAP
+V12Rac1
+199AA
+V12Rac1
+MgcRacGAP
+V12Rac1
+importin α1
+importin β1
+Ran
+NTF2
+199AA
+V12Rac1
+importin α1
+importin β1
+Ran
+NTF2
a
b
c
d
e
+STAT5A
f
g
h
i
j
+p-STAT5A

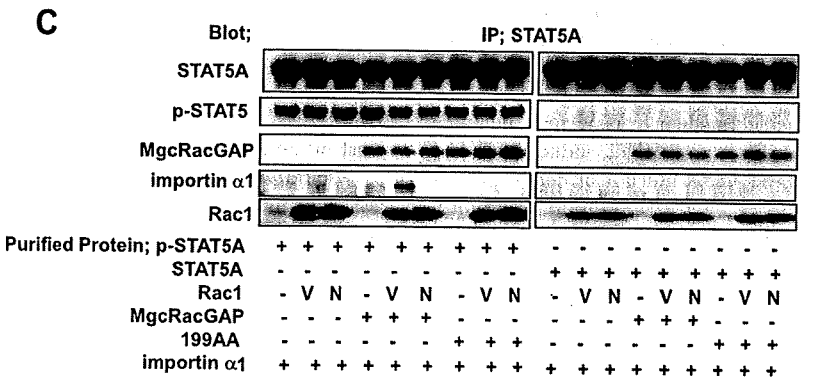
C
Blot;
IP; STAT5A
STAT5A
p-STAT5
MgcRacGAP
importin α1
Rac1
Purified Protein; p-STAT5A + + + + + + + + + - - - - - - - - -
STAT5A - - - - - - - - - + + + + + + + + +
Rac1 - V N - V N - V N - V N - V N - V N
MgcRacGAP - - - + + + - - - - - - + + + - - -
199AA - - - - - - + + + - - - - - - + + +
importin α1 + + + + + + + + + + + + + + + + + +

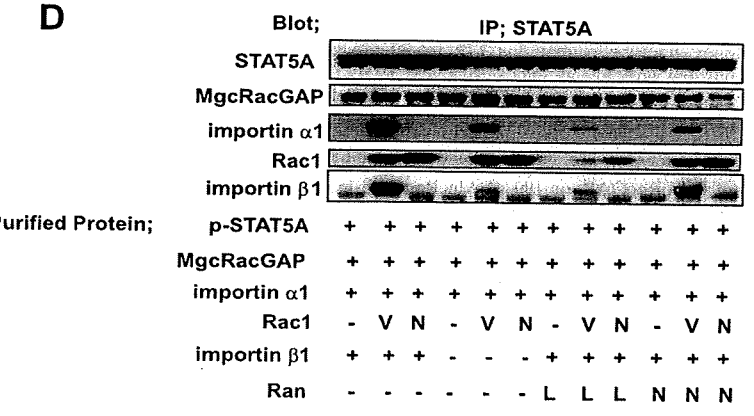
D
Blot;
IP; STAT5A
STAT5A
MgcRacGAP
importin α1
Rac1
importin β1
Purified Protein;
p-STAT5A + + + + + + + + + + + +
MgcRacGAP + + + + + + + + + + + +
importin α1 + + + + + + + + + + + +
Rac1 - V N - V N - V N - V N
importin β1 + + + - - - + + + + + +
Ran - - - - - - L L L N N N

GAP directly bound importin αs through its bipartite NLS (182KRR and 199KK).

NLSs of MgcRacGAP and GTP-bound Rac1 were required for nuclear translocation of p-STATs in the in vitro nuclear transport assay. GTP-bound Rac1 and MgcRacGAP were reported to promote nuclear translocation of p-STATs, forming a ternary complex via the importin α/β pathway in an in vitro nuclear transport assay (17), but the component of the ternary complex that directly binds importin α remained elusive. Neither STAT3 nor STAT5 harbors an apparent polybasic or PY-type NLS. One possibility is that p-STATs themselves harbor unidentified functional NLSs. However, the requirement of MgcRacGAP/GTP-Rac1 for the nuclear translocation of p-STATs raises another possibility that MgcRacGAP functions as an NLS-containing nuclear chaperone of p-STATs. We first asked if the NLS of MgcRacGAP plays a role in the nuclear translocation of p-STAT5A by using an in vitro nuclear transport assay (1). For this, Sf-9-mediated protein purification was done for WT or the 199AA mutant of MgcRacGAP, a constitutively active mutant Rac1 (V12Rac1), STAT5A, or p-STAT5A and for nuclear transporter proteins, including importin α1, importin β1, Ran, and NTF2, which binds Ran and enhances Ran-dependent nuclear import (Fig. 2A, panel a). We confirmed the purities of recombinant proteins and the tyrosine phosphorylation of STAT5A induced by coexpression with the kinase domain of JAK2 (JH1) (40) in Sf-9 cells (Fig. 2A, panels a and b). We also examined the extent of STAT5A phosphorylation by phosphate-affinity SDS-PAGE using acrylamide-pendant Phos-tag and found that about 10% was phosphorylated by coexpression of JH1 (data not shown). Although purified p-STAT5A contained only about 10% phosphorylated forms, as we previously reported (17), efficient accumulation to the nuclear envelope of p-STAT5A but not of unphosphorylated STAT5A was achieved in the presence of both purified MgcRacGAP and V12Rac1 (Fig. 2B, panels g and b), and further addition of the purified nuclear transporters, including importin α1, importin β1, Ran, and NTF2, induced efficient nuclear translocation of p-STAT5A but not of unphosphorylated STAT5A (Fig. 2B, panels i and d). Addition of the purified nuclear transporters alone was not sufficient for the nuclear translocation of p-STAT5A, and the addition of purified dominant negative N17Rac1 instead of V12Rac1 blocked the nuclear translocation of p-STAT5A even in the presence of purified MgcRacGAP and other nuclear transporters (data not shown). Notably, 199AA-MgcRacGAP did not support the accumulation of p-STAT5A at the nuclear envelope, even in the presence of V12Rac1, and abolished the nuclear translocation of p-STAT5A even in the presence of V12Rac1, importin α1, importin β1, Ran, and NTF2 (Fig. 2B, panels h and j).

To determine if both the NLS of MgcRacGAP and Rac1 activation are required for complex formation of p-STAT5A with importin α, an in vitro binding assay was done. As we reported previously (17), p-STAT5A, but not unphosphorylated STAT5A, formed complexes with importin α1 only in the presence of WT MgcRacGAP and V12Rac1 (Fig. 2C). On the other hand, p-STAT5A did not form complexes with importin α1 in the presence of 199AA-MgcRacGAP and V12Rac1 (Fig. 2C). Addition of importin β1 increased the amount of importin α1 associating with the complex of p-STAT5A, WT MgcRacGAP, and V12Rac1, and further addition of GTP-bound Ran (L69Ran) but not GDP-bound Ran (N24Ran) dissociated the import complex (Fig. 2D), suggesting that Ran was indeed involved in the nuclear import of p-STAT5A. We also found that 199AA-MgcRacGAP did not support the nuclear translocation of p-STAT3 in the presence of V12Rac1, importin α1, importin β1, Ran, or NTF2 (see Fig. S2 in the supplemental material). Conversely, addition of purified p-STATs and V12Rac1 was required for the nuclear import of GST-MgcRacGAP in the presence of purified importin α/β pathway proteins (see Fig. S3A and B in the supplemental material). These results suggested that the NLS of MgcRacGAP was somehow activated by the association with p-STATs and GTP-bound Rac1, and bound importin α, thereby facilitating nuclear transport of the MgcRacGAP/p-STATs/Rac1 complex. Altogether, the present results indicate that the bipartite NLS was essential for MgcRacGAP to function as a nuclear chaperone of p-STATs, in accordance with GTP-bound Rac1, at least in the in vitro nuclear transport assay.

Generation of MgcRacGAP conditional knockout DT40 cells, in which expression of exogenous MgcRacGAP is under control of a tetracycline-repressible promoter. To determine if the 199AA or 182AAA/199AA mutant could alter the tran-

FIG. 2. Nuclear translocation of p-STAT5A requires the NLS of MgcRacGAP. (A) The recombinant proteins used in the experiments are shown, after CBB staining of purified proteins (a) or Western blot analysis of the STAT5A-Flag protein purified from Sf-9 cells with or without coexpression with the kinase domain of JAK, using the anti-p-STAT5 Ab (b). (B) Nuclear transport assay of STAT5A. HeLa cells were permeabilized using 40 μg/ml digitonin and were incubated at 37°C for 30 min with 50 μl IM. The IM contained TB, ERS, and a single protein or combinations of the following purified proteins, as indicated: 1 μM STAT5A, p-STAT5A, V12Rac1, MgcRacGAP, 199AA-MgcRacGAP, importin α1, importin β1, Ran, or NTF2. After the import reaction, the cells were fixed. STAT5A protein was detected using the anti-STAT5A Ab. Cells were examined using a FLUOVIEW FV300 confocal microscope (Olympus). A representative result of three independent experiments is shown. Bar, 10 μm. (C) The ternary protein complex composed of p-STAT5A, GTP-bound Rac1, and 199AA-MgcRacGAP did not bind importin α1 in the transport buffer. Purified STAT5A and p-STAT5A were incubated with importin α1 in the absence or presence of the indicated combinations of V12Rac1, N17Rac1, MgcRacGAP, or 199AA-MgcRacGAP in the transport buffer containing 5% bovine serum albumin for blocking nonspecific binding. One microgram of each purified protein was used for each sample. After the incubation, STAT5A was immunoprecipitated (IP) with anti-STAT5A Ab and washed three times with transport buffer. The immunoprecipitates were subjected to Western blot analysis with the anti-importin α1, anti-Rac1, anti-MgcRacGAP, anti-STAT5A Ab, or anti-p-STAT5A Ab. (D) GTP-bound Ran (L69Ran) dissociates Rac1, importin α1, and importin β1 from the import complex composed of p-STAT5A. Purified p-STAT5A was incubated with purified V12Rac1, MgcRacGAP, and importin α1 in the presence of the indicated combinations of purified importin β1 alone, importin β1 plus Q69Ran (GTP-bound Ran), or importin β1 plus N24Ran (GDP-bound Ran) in the transport buffer containing 5% bovine serum albumin for blocking nonspecific binding. One microgram of each purified protein was used for each sample. After the incubation, STAT5A was immunoprecipitated with anti-STAT5A Ab and washed three times with transport buffer. The immunoprecipitates were subjected to Western blot analysis with the anti-importin α1, anti-Rac1, anti-MgcRacGAP, anti-importin β1, or anti-STAT5A Ab.

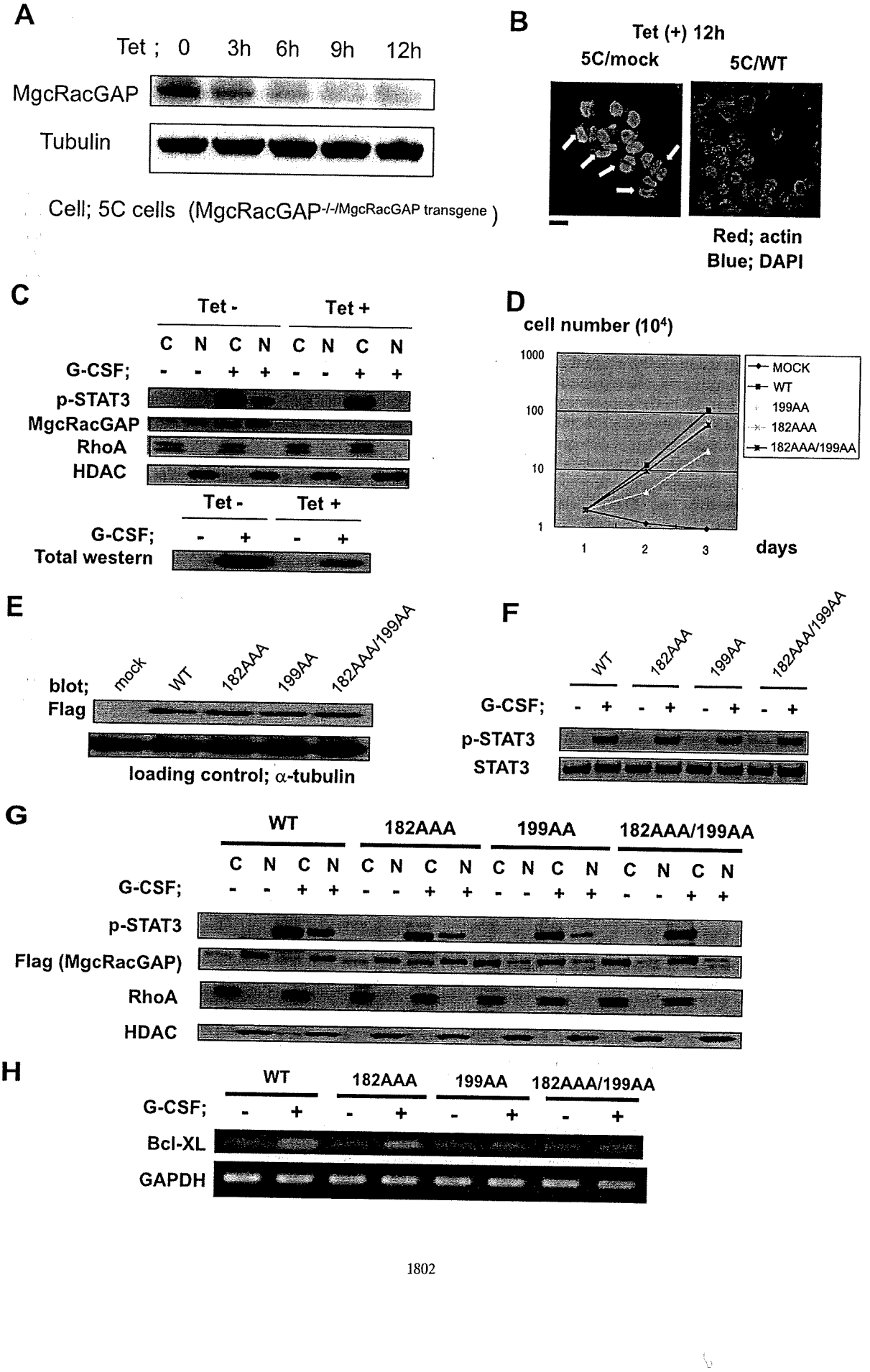
A
Tet ; 0 3h 6h 9h 12h
MgcRacGAP
Tubulin
Cell; 5C cells (MgcRacGAP-/-/MgcRacGAP transgene)
B
Tet (+) 12h
5C/mock
5C/WT
Red; actin
Blue; DAPI
C
Tet - Tet +
C N C N C N C N
G-CSF; - - + + - - + +
p-STAT3
MgcRacGAP
RhoA
HDAC
Tet - Tet +
G-CSF; - + - +
Total western
D
cell number (10^4)
1000
100
10
1
1 2 3
days
MOCK
WT
199AA
182AAA
182AAA/199AA
E
blot; mock WT 182AAA 199AA 182AAA/199AA
Flag
loading control; α-tubulin
F
WT 182AAA 199AA 182AAA/199AA
G-CSF; - + - + - + - +
p-STAT3
STAT3
G
WT 182AAA 199AA 182AAA/199AA
C N C N C N C N C N C N C N C N
G-CSF; - - + + - - + + - - + + - - + +
p-STAT3
Flag (MgcRacGAP)
RhoA
HDAC
H
WT 182AAA 199AA 182AAA/199AA
G-CSF; - + - + - + - +
Bcl-XL
GAPDH

scriptional activation of STATs in vivo, we first performed a luciferase assay using 293T cells. The IL-6-induced activation of STAT3 was clearly enhanced by cotransfection with the wild-type MgcRacGAP (~45-fold, compared with mock transfection [~10-fold]). Unexpectedly, cotransfection of the 199AA or 182AAA/199AA mutant modestly inhibited the IL-6-induced transactivation of STAT3 (~25-fold) compared with WT but, rather, enhanced it when compared with mock treatment (data not shown). It is possible that these MgcRacGAP mutants form a heterodimer with endogenous MgcRacGAP and that the heterodimer but not the homodimer of the 199AA or 182AAA/199AA mutant enhanced IL-6-induced transcriptional activation of STAT3. To exclude the effects of endogenous MgcRacGAP, we attempted to establish an MgcRacGAP conditional knockout using DT40 cells. We generated DT40 mutants in which cells with a disrupted MgcRacGAP gene were sustained by expression of the exogenous MgcRacGAP cDNA under the control of a tetracycline-repressible promoter. As shown in Fig. S4A in the supplemental material, an MgcRacGAP-targeting construct was generated such that the 8.0-kb genomic fragment encoding the open reading frame was replaced with one of the two selection cassettes. We transfected the MgcRacGAP-targeting construct containing the histidinol resistance cassette into DT40 cells and isolated MgcRacGAP$^{+/-}$ clones. One MgcRacGAP$^{+/-}$ clone was cotransfected with a chicken MgcRacGAP transgene under the control of a TET-repressible promoter and a TET-repressible transactivator containing a zeocin (ZEO) resistance cassette. We selected ZEO-resistant colonies and identified several clones carrying these constructs integrated at random sites in the genome (MgcRacGAP$^{+/-/\text{MgcRacGAP transgene}}$). Five clones with the MgcRacGAP$^{+/-/\text{MgcRacGAP transgene}}$ genotype were transfected with another MgcRacGAP-targeting construct harboring a puromycin selection marker to disrupt the remaining MgcRacGAP allele. We obtained 24 clones with the MgcRacGAP$^{-/-/\text{MgcRacGAP transgene}}$ genotype, and one clone, 5C, was chosen for further analysis (see Fig. S4B, panels a and b, in the supplemental material). Exogenous MgcRacGAP protein under the control of a TET-repressible promoter in 5C cells was not detected by Western blot analysis with anti-chicken MgcRacGAP Ab at 6 to 12 h after addition of TET, indicating that a TET-repressible promoter of this clone worked successfully and that MgcRacGAP was actively turned over (Fig. 3A). When the expression of the MgcRacGAP transgene was suppressed by adding TET, cell growth of 5C cells was suppressed together with the inhibition of cytokinesis, and the cells formed multinucleated cells, eventually undergoing apoptosis within 48 h (Fig. 3B and data not shown). This phenotype is consistent with the previous result indicating that MgcRacGAP is required for completion of cytokinesis.

The 199AA and 182AAA/199AA mutants inhibited nuclear translocation and transcriptional activation of p-STAT3 in MgcRacGAP knockout cells. To determine if MgcRacGAP is required for the nuclear translocation of p-STAT3 in vivo, we investigated whether depletion of MgcRacGAP affected the subcellular distribution of p-STAT3 after granulocyte colony-stimulating factor (G-CSF) stimulation using the 5C cells. The 5C cells, which had been transiently transfected with a vector carrying a G-CSF receptor, were treated with TET for 4 h and were stimulated with G-CSF (15 min), followed by nuclear-cytosol fractionation analysis. We also confirmed that after treatment with TET for 4 h only a portion of the 5C cells formed multinucleated cells (less than 10%) (data not shown). The nuclear-cytosol fractionation analysis revealed that depletion of MgcRacGAP resulted in a decreased amount of the G-CSF-induced p-STAT3 as well as inhibition of the nuclear accumulation of p-STAT3 (Fig. 3C). These results implied that MgcRacGAP mediates the G-CSF-induced phosphorylation

FIG. 3. The NLS of MgcRacGAP is required for the transcriptional activation of p-STAT3 in 5C cells. (A) Suppression of MgcRacGAP by TET in 5C cells. The 5C cells were treated with TET for the time indicated and lysed. Cell lysates were separated on SDS-PAGE and immunoblotted with the anti-chicken MgcRacGAP Ab (upper panel) or anti-α-tubulin Ab (lower panel). (B) Flag-tagged WT MgcRacGAP rescued 5C cells from becoming multinucleated after addition of TET. The 5C cells transduced with mock or Flag-tagged WT were stained with rhodamine-conjugated phalloidin (red) and DAPI (blue) 12 h after the addition of TET and viewed using a FLUOVIEW FV300 confocal microscope (Olympus). Bar, 10 μm. (C) Subcellular localization of p-STAT3 in 5C cells after addition of TET in the absence or presence of G-CSF. Cell fractionation was performed using 5C cells transiently transfected with the expression vector for the G-CSF receptor (G-CSFR). Twenty-four hours after transfection, live cells were isolated using Ficoll-Paque Plus (Amersham) and used for further analysis. Cells were treated or untreated with TET for 4 h and were incubated with 100 ng/ml of G-CSF for 15 min before cell fractionations. Fractionated samples were then subjected to Western blotting with anti-p-STAT3, anti-Flag, anti-RhoA, or anti-HDAC Ab (upper panels). The total amount of p-STAT3 was also examined using whole-cell lysates of 5C cells by Western blotting with anti-p-STAT3 (lower panel). C, cytosol; N, nuclear. (D) Effect of NLS mutants of MgcRacGAP on cell proliferation. Flag-tagged WT or various MgcRacGAP mutants (182AAA, 199AA, and 182AAA/199AA) were transduced into 5C cells by using a retrovirus vector, pMXs-IG. GFP-positive cells were selected by addition of TET. The number of transfectants was counted at the indicated time points after selection. GFP-positive mock-transduced cells, which were analyzed using fluorescence-activated cell sorting, were used as a control. (E) Expression levels of the Flag-tagged WT or mutant MgcRacGAPs in 5C transfectants. Cell lysates from 5C cells expressing mock, WT, or mutant MgcRacGAPs (1×10^7/lane) were examined by Western blotting using the anti-Flag M2 monoclonal antibody (upper panel) or anti-α-tubulin Ab (lower panel). (F) G-CSF-induced phosphorylation of STAT3 in 5C cells expressing Flag-tagged WT or mutant MgcRacGAPs. The 5C cells expressing WT or mutant MgcRacGAPs cotransfected with the expression vector for G-CSFR were stimulated with 100 ng/ml of G-CSF for 15 min in the presence of TET, followed by Western blotting (5×10^6 cells/lane) using the anti-p-STAT3 antibody (upper panel) or anti-STAT3 Ab (lower panel). (G) Subcellular localization of p-STAT3 in 5C cells expressing Flag-tagged WT, 182AAA, 199AA, or 182AAA/199AA with or without G-CSF stimulation in the presence of TET. Cell fractionation was performed using 5C transfectants cotransfected with the expression vector for G-CSFR. Twenty-four hours after transfection, live cells were isolated using Ficoll-Paque Plus (Amersham) and used for further analysis. Cells were incubated with 100 ng/ml of G-CSF for 15 min before cell fractionations. Fractionated samples were then subjected to Western blotting with anti-p-STAT3, anti-Flag, anti-RhoA, or anti-HDAC Ab. (H) G-CSF-induced transcriptional activation of STAT3 was suppressed by depletion of MgcRacGAP. Expression of Bcl-xL or GAPDH mRNA was examined in the 5C transfectants expressing WT, 182AAA, 199AA, or 182AAA/199AA with or without G-CSF stimulation. Cells transiently transfected with G-CSFR were serum starved with or without G-CSF stimulation for 7 h in the presence of TET, followed by semiquantitative RT-PCR.

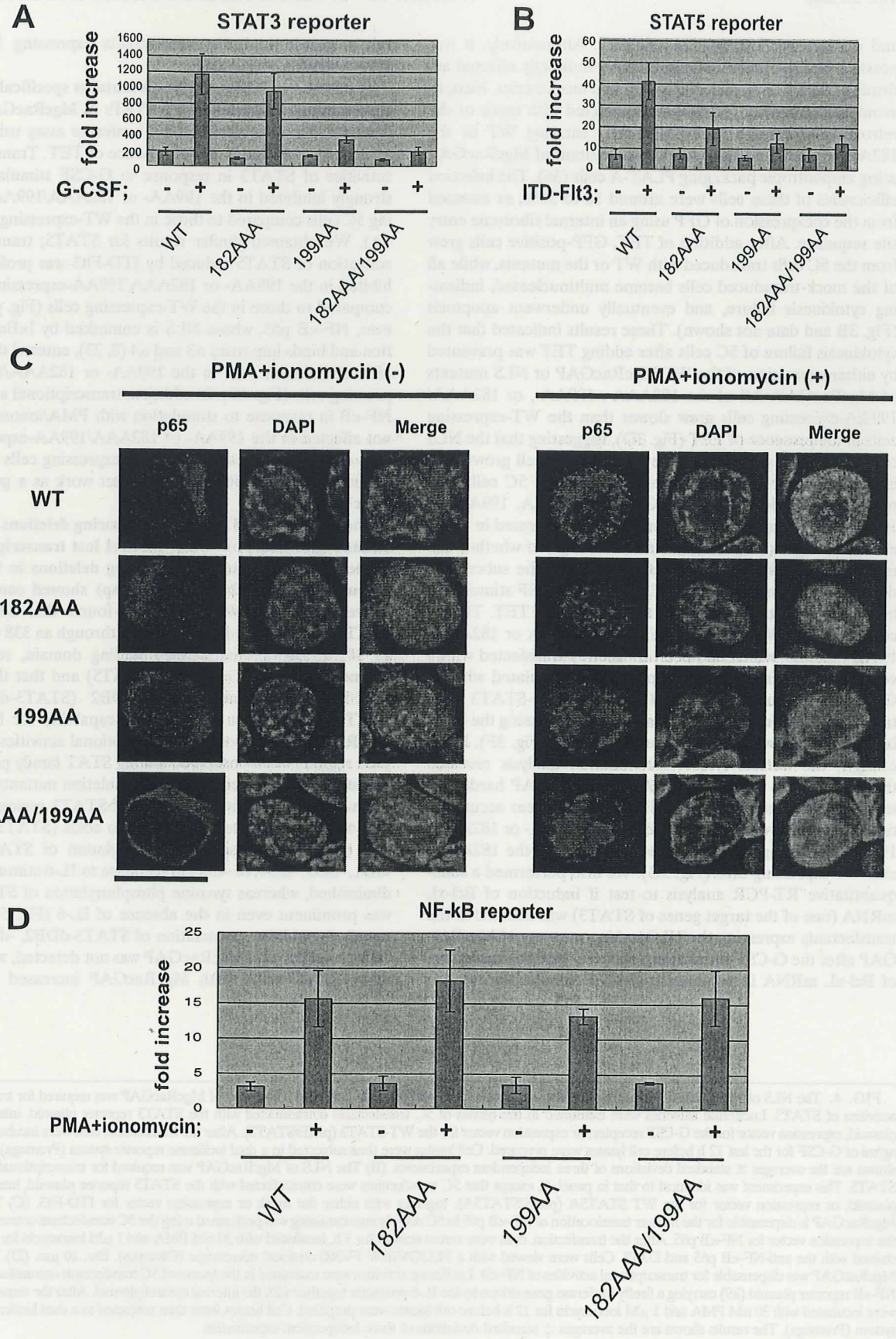
A
STAT3 reporter
fold increase
1600
1400
1200
1000
800
600
400
200
0
G-CSF; - + - + - + - +
WT
182AAA
199AA
182AAA/199AA
B
STAT5 reporter
fold increase
60
50
40
30
20
10
0
ITD-Flt3; - + - + - + - +
WT
182AAA
199AA
182AAA/199AA
C
PMA+ionomycin (-)
PMA+ionomycin (+)
p65
DAPI
Merge
WT
182AAA
199AA
182AAA/199AA
D
NF-kB reporter
fold increase
25
20
15
10
5
0
PMA+ionomycin; - + - + - + - +
WT
182AAA
199AA
182AAA/199AA

and nuclear translocation of p-STAT3. Alternatively, it was possible that depletion of MgcRacGAP indirectly affected activation of STAT3 by disturbing cell cycle machineries. Next, to avoid this possibility, 5C cells were infected with mock or the retrovirus expression vector pMXs-IG carrying WT or the 182AAA, 199AA, or 182AAA/199AA mutant of MgcRacGAP using amphotropic packaging PLAT-A cells (36). The infection efficiencies of these cells were around 10 to 30%, as assessed from the coexpression of GFP using an internal ribosome entry site sequence. After addition of TET, GFP-positive cells grew from the 5C cells transduced with WT or the mutants, while all of the mock-transduced cells became multinucleated, indicating cytokinesis failure, and eventually underwent apoptosis (Fig. 3B and data not shown). These results indicated that the cytokinesis failure of 5C cells after adding TET was prevented by either expression of the WT MgcRacGAP or NLS mutants of MgcRacGAP. All of the 182AAA-, 199AA-, or 182AAA/199AA-expressing cells grew slower than the WT-expressing cells in the presence of TET (Fig. 3D), suggesting that the NLS of MgcRacGAP plays some role in enhancing cell growth but is dispensable for completion of cytokinesis in 5C cells. Expression levels of WT MgcRacGAP or 182AAA, 199AA, or 182AAA/199AA mutant were comparable as assessed in Western blot analyses (Fig. 3E). We next investigated whether disruption of the NLS of MgcRacGAP affected the subcellular distribution of endogenous p-STAT3 after G-CSF stimulation by using the 5C transfectants in the presence of TET. The 5C cells expressing WT MgcRacGAP or the 199AA or 182AAA/199AA mutant, which had been transiently transfected with a vector carrying the G-CSF receptor, were stimulated with G-CSF (15 min). The amounts of G-CSF-induced p-STAT3 in 5C transfectants expressing the WT and those expressing the NLS-lacking mutants were found to be comparable (Fig. 3F). Interestingly, the nuclear-cytosol fractionation analysis revealed that the 199AA- or 182AAA/199AA-MgcRacGAP hardly entered the nucleus, and the G-CSF-induced nuclear accumulation of p-STAT3 was strongly inhibited in 199AA- or 182AAA/199AA-expressing cells compared with those in the 182AAA- and WT-expressing cells (Fig. 3G). We also performed a semiquantitative RT-PCR analysis to test if induction of Bcl-xL mRNA (one of the target genes of STAT3) was affected in the transfectants expressing the NLS-lacking mutants of MgcRacGAP after the G-CSF stimulation, and we found that induction of Bcl-xL mRNA in response to G-CSF stimulation was severely impaired in the transfectants expressing 199AA or 182AAA/199AA (Fig. 3H).

The 199AA and 182AAA/199AA mutants specifically blocked transcriptional activation of p-STATs in MgcRacGAP knockout cells. Next, we performed a luciferase assay using the 5C transfectants cultured in the presence of TET. Transcriptional activities of STAT3 in response to G-CSF stimulation were strongly inhibited in the 199AA- or 182AAA/199AA-expressing 5C cells compared to those in the WT-expressing cells (Fig. 4A). We obtained similar results for STAT5; transcriptional activation of STAT5 induced by ITD-Flt3 was profoundly inhibited in the 199AA- or 182AAA/199AA-expressing 5C cells compared to those in the WT-expressing cells (Fig. 4B). However, NF-κB p65, whose NLS is unmasked by IκBα degradation and binds importins α3 and α4 (8, 23), entered the nucleus after stimulation even in the 199AA- or 182AAA/199AA-expressing cells (Fig. 4C). In addition, transcriptional activities of NF-κB in response to stimulation with PMA/ionomycin were not affected in the 199AA- or 182AAA/199AA-expressing 5C cells compared to those in the WT-expressing cells (Fig. 4D), indicating that MgcRacGAP does not work as a general nuclear chaperone.

The series of STAT3 mutants harboring deletions in the two strands (βa′ and βb) of the β-barrel lost transcriptional activities, while the mutants harboring deletions in the region following the strand βb (βb-βc loop) showed constitutively active phenotypes. We previously found that STAT3 and STAT5 directly bound MgcRacGAP through aa 338 to 362 and aa 341 to 365 in their DNA binding domain, respectively (termed DB2-STAT3 and DB2-STAT5) and that the STAT3 and STAT5A mutants lacking DB2 (STAT3-dDB2 and STAT5A-dDB2) lost not only the capability for binding to MgcRacGAP but also their transcriptional activities (17). The DB2 region is well-conserved among STAT family proteins. In this study, we produced a series of deletion mutants lacking a three-amino-acid stretch in the DB2-STAT3 region (STAT3-dD1 to -8) and in the next six amino acids (STAT3-dD9 and -10) (Fig. 5A). Tyrosine phosphorylation of STAT3-dDB2, -dD1, -dD3, -dD4, or -dD5 in response to IL-6 stimulation was diminished, whereas tyrosine phosphorylation of STAT3-dD2 was prominent even in the absence of IL-6 (Fig. 5C, middle panel). In addition, association of STAT3-dDB2, -dD1, -dD3, -dD4, or -dD5 with MgcRacGAP was not detected, while binding of STAT3-dD2 with MgcRacGAP increased compared

FIG. 4. The NLS of MgcRacGAP is not required for activation of NF-κB p65 in 5C cells. (A) The NLS of MgcRacGAP was required for transcriptional activities of STAT3. Luciferase activities were examined in the lysates of 5C transfectants cotransfected with the STAT3 reporter plasmid, internal control plasmid, expression vector for the G-CSF receptor, or expression vector for the WT-STAT3 (pME/STAT3). After the transfection, cells were incubated with 100 ng/ml of G-CSF for the last 12 h before cell lysates were prepared. Cell lysates were then subjected to a dual luciferase reporter system (Promega). The results shown are the averages ± standard deviations of three independent experiments. (B) The NLS of MgcRacGAP was required for transcriptional activities of STAT5. This experiment was identical to that in panel A, except that 5C transfectants were cotransfected with the STAT5 reporter plasmid, internal control plasmid, or expression vector for the WT STAT5A (pME/STAT5A), together with either the mock or expression vector for ITD-Flt3. (C) The NLS of MgcRacGAP is dispensable for the nuclear translocation of NF-κB p65 in 5C cells. Immunostaining was performed using the 5C transfectants cotransfected with the expression vector for NF-κB p65. After the transfection, cells were serum starved for 3 h, incubated with 30 nM PMA and 1 μM ionomycin for 30 min, and stained with the anti-NF-κB p65 and DAPI. Cells were viewed with a FLUOVIEW FV300 confocal microscope (Olympus). Bar, 10 μm. (D) The NLS of MgcRacGAP was dispensable for transcriptional activities of NF-κB. Luciferase activities were examined in the lysates of 5C transfectants cotransfected with the NF-κB reporter plasmid (k9) carrying a firefly luciferase gene driven by the IL-6 promoter together with the internal control plasmid. After the transfection, cells were incubated with 30 nM PMA and 1 μM ionomycin for 12 h before cell lysates were prepared. Cell lysates were then subjected to a dual luciferase reporter system (Promega). The results shown are the averages ± standard deviations of three independent experiments.

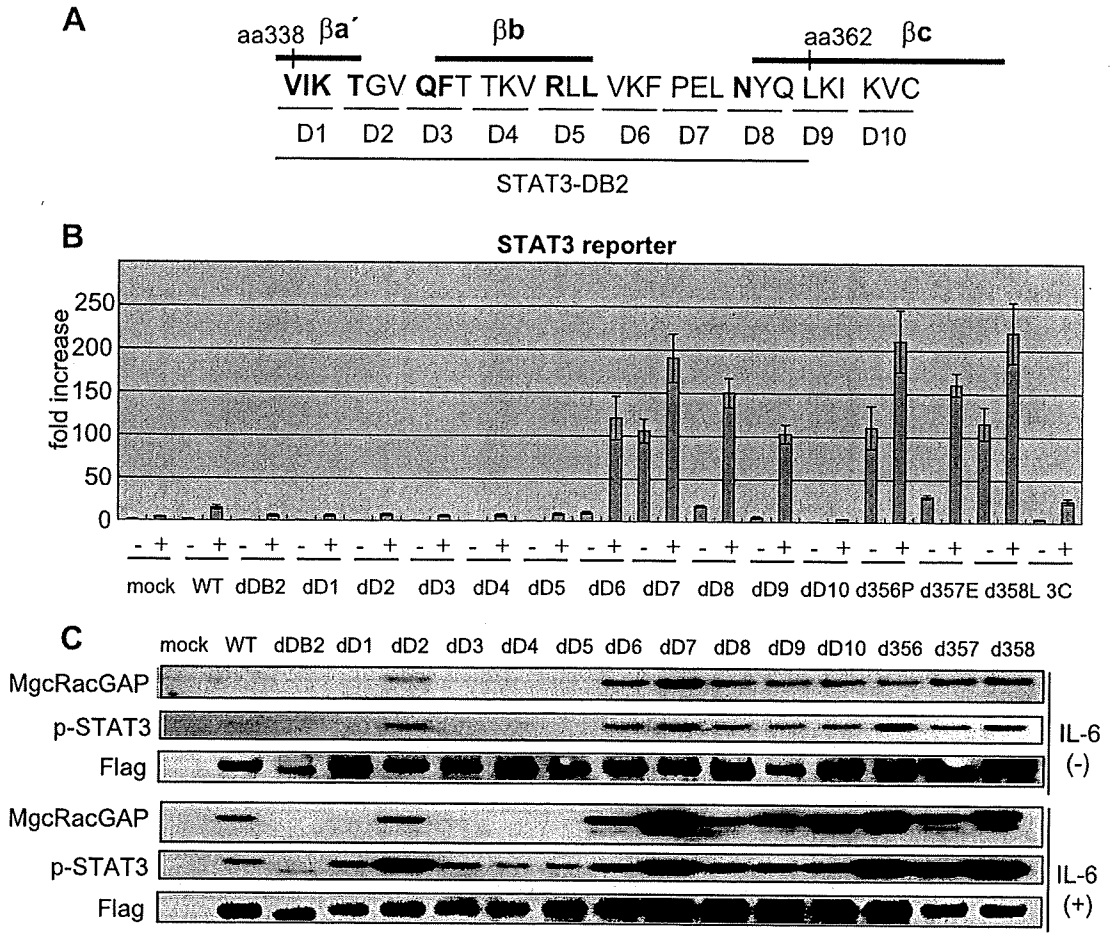

FIG. 5. Correlation between binding abilities of STAT3 to MgcRacGAP and activities of STAT3. (A) Schematic diagrams showing a series of the deletion sites of STAT3 mutants. (B) Transcriptional activities of STAT3 mutants harboring deletions in DB2. Luciferase activity was examined as described in Materials and Methods. As a control, a reported constitutively active mutant of STAT3C was used. The results shown are the averages ± standard deviations of three independent experiments. (C) MgcRacGAP binding abilities of the STAT3 mutants. Tyrosine phosphorylation and binding affinity to MgcRacGAP of Flag-tagged deletion mutants of DB2-STAT3 in the absence or presence of IL-6-stimulation were determined by immunoprecipitation using the anti-Flag Ab followed by Western blotting with the anti-p-STAT3, anti-MgcRacGAP, or anti-Flag Ab. Expression, tyrosine phosphorylation, and interaction with MgcRacGAP of the Flag-tagged deletion mutants of DB2-STAT3 (lower panel, middle panel, and upper panel, respectively) were examined by immunoprecipitation using 293T cells transfected with each of the STAT3 mutants in the absence (upper three panels) or presence (lower three panels) of IL-6-stimulation for 30 min.

with that of WT in the absence or presence of IL-6 stimulation (Fig. 5C, upper panels). Nonetheless, the mutants lacking D1 to -5 (STAT3-dD1 to -5), including STAT3-dD2, did not show detectable transcriptional activities in response to IL-6 stimulation (Fig. 5B). Surprisingly, STAT3-dD6 to -9 mutants exerted considerable transcriptional activities even without cytokine stimulation, and this was further enhanced by IL-6 stimulation (Fig. 5B). These mutants were constitutively tyrosine phosphorylated, and their tyrosine phosphorylation was augmented after IL-6 stimulation (Fig. 5C). STAT3-dD10 was constitutively tyrosine phosphorylated but did not show detectable transcriptional activities, as was the case for STAT3-dD2. We next examined whether these STAT3 mutants harbored the DNA binding activities in an electrophoretic mobility shift assay using unstimulated 293T cells and found that unlike the other constitutively tyrosine-phosphorylated STAT3 mutants, STAT3-dD2 and STAT3-dD10 lost their DNA binding affinities (data not shown). Notably, STAT3-dD7 showed the strongest transcriptional activities in the absence of cytokine stimulation among the STAT3-dD1 to -10 mutants, and its transcriptional activities in the absence of cytokine stimulation were much stronger than that of the WT after IL-6 stimulation (Fig. 5B). We next produced a series of mutants lacking each single amino acid of the three amino acids in the region of D7 (STAT3-d356P, -d357E, and -d358L). Interestingly, STAT3-d356P, -d357E, and -d358L, which strongly bound MgcRacGAP, displayed the constitutive activities in the absence of IL-6 stimulation (Fig. 5B and C). STAT3-d356P and STAT3-d358L exerted the strongest transcriptional activity among these mutants and a reported constitutively active mutant of STAT3C (3). These results suggest that the two strands (βa′ and βb) in DB2 are required for the IL-6-induced tyrosine phosphorylation of STAT3 that mediates the interaction with MgcRacGAP, whereas the deletion mutants in the C terminus

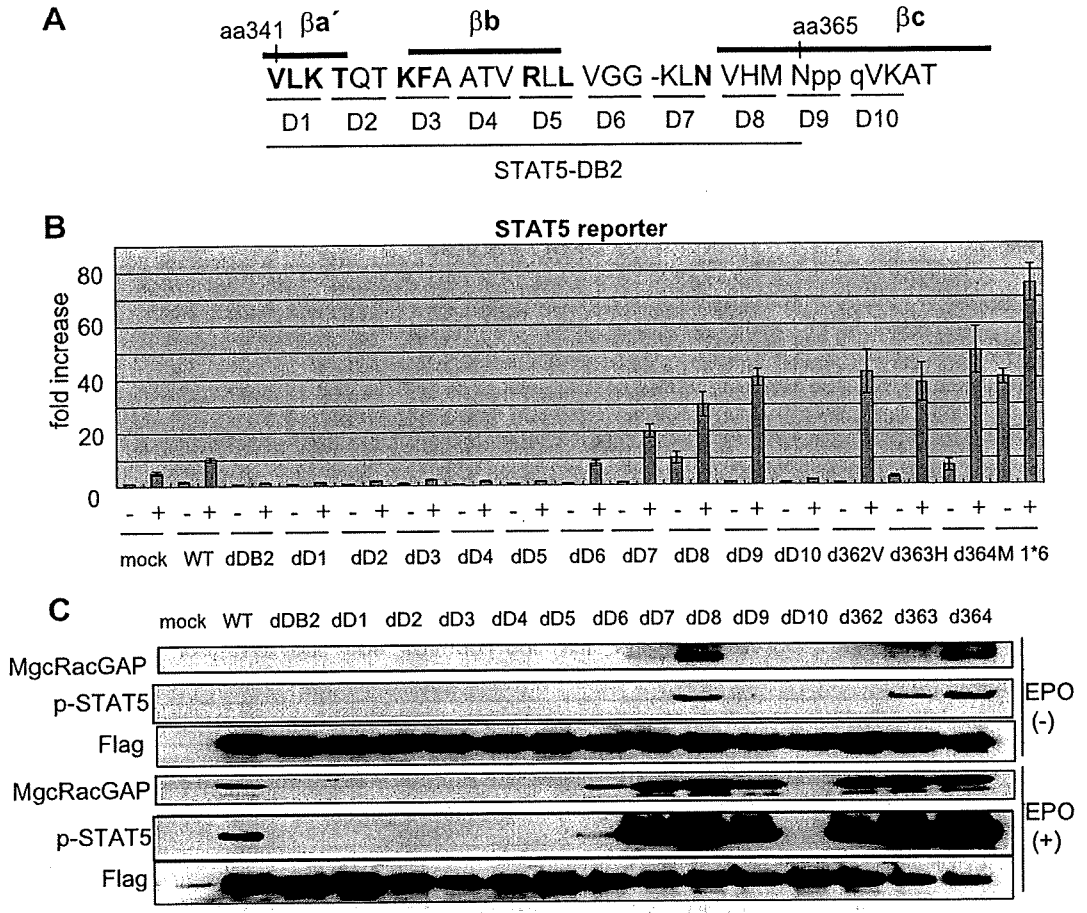

FIG. 6. The series of deletion mutants of STAT5A in DB2 showed similar phenotypes to those of STAT3. (A) Schematic diagrams showing a series of the deletion mutants of STAT5A. (B) The mutants lacking D1 to -5 and D10 (STAT5A-dD1 to -5 and STAT5A-dD10) as well as the STAT5A-dDB2 lacked their transcriptional activities even under EPO stimulation. Luciferase activity was examined in the lysates of unstimulated or EPO (18 ng/ml)-stimulated 293T cells cotransfected with the expression vector for the EPO receptor (EPOR) and STAT5 reporter plasmid together with internal control reporter plasmids and either the mock vector (pME), the expression vector for the Flag-tagged WT STAT5A, or a series of STAT5A mutants harboring deletions in DB2. As a control, the constitutively active STAT5A1*6 mutant was used. The results shown are the averages ± standard deviations of three independent experiments. (C) The mutants of STAT5A harboring deletions in the two strands (βaprime] and βb) lost binding affinities to MgcRacGAP or did not undergo tyrosine phosphorylation, while the mutants harboring deletions in the region following the strand βb showed enhanced binding affinities to MgcRacGAP and underwent enhanced tyrosine phosphorylation. Expression, tyrosine phosphorylation, and interaction with MgcRacGAP of the Flag-tagged deletion mutants of DB2-STAT5A (lower panel, middle panel, and upper panel, respectively) were examined by immunoprecipitation using 293T cells cotransfected with EPOR and each of the STAT5A mutants in the absence (upper three panels) or presence (lower three panels) of EPO stimulation for 30 min.

of DB2 following the strand βb (βb-βc loop) tend to become constitutively active with enhanced binding to MgcRacGAP.

We also produced a series of STAT5A mutants lacking a three-amino-acid stretch in the region corresponding to DB2-STAT3 (STAT5A-dD1 to -8) and in the next six amino acids (STAT5A-dD9 and -10) (Fig. 6A). We found that the series of deletion mutants of STAT5A in DB2 showed phenotypes similar to those of STAT3 mutants (Fig. 6B and C); STAT5A mutants harboring deletions in the two strands (βa′ and βb) of the β-barrel (STAT5A-dD1 to -5) were not tyrosine phosphorylated by EPO stimulation and lost transcriptional activity, while the mutants harboring deletions in the region following the strand βb (STAT5A-dD7 to -9) showed gain-of-function phenotypes. STAT5A-dD8, -d363H, and -d364M also showed constitutively active phenotypes (Fig. 6B and C), although the transcriptional activities of these mutants without stimulation were weaker than that of another constitutively active mutant, STAT5A1*6 (37). Constitutive activities of STAT5A mutants were well-correlated with constitutive binding to MgcRacGAP. Association between the constitutively active STAT5A mutants and MgcRacGAP was stronger than that of the WT and MgcRacGAP in the absence of EPO stimulation (Fig. 6C). Thus, the molecular basis of the STAT-MgcRacGAP interaction is well-conserved between STAT3 and STAT5A.

The constitutively active mutant STAT3-d358L promoted cell proliferation of a mutant cell line derived from BaF-BO3 cells. We next examined whether STAT3-d358L was biologically functional, showing physiological roles of STAT3 activation. It has been reported that BaF-BO3 cells expressing a G-CSF receptor mutant (G133 cells) are able to proliferate in

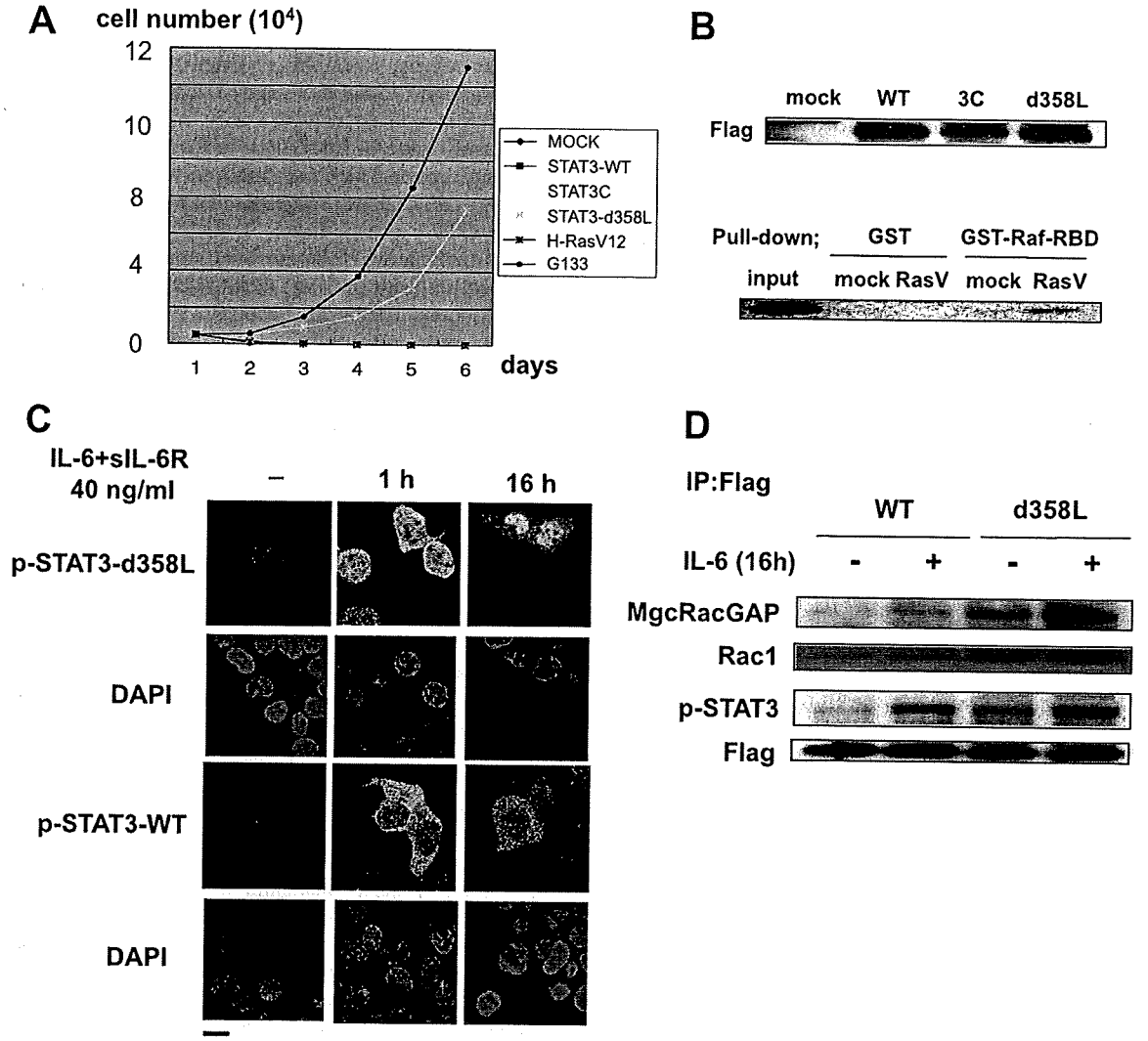

FIG. 7. A constitutively active STAT3 mutant, STAT3-d358L, preferentially bound MgcRacGAP and Rac1 and accumulated to the nucleus. (A) STAT3-d358L supports proliferation of BaF-BO3-G133F3 cells in the presence of G-CSF. BaF-BO3-G133F3 cells expressing mock vector or the Flag-tagged WT STAT3, STAT3C, STAT3-d358L, or H-RasV12 were cultured in the presence of G-CSF, and the cell numbers were determined at the indicated times. BaF-BO3-G133 cells were used as a control. (B) Similar expression levels of WT STAT3, STAT3C, and STAT3-d358L were confirmed by Western blotting with the anti-Flag Ab (upper panel). The expression and activation of H-RasV12 were examined by Western blotting with the anti-Flag Ab (lower panel; input lane) and by pull-down assay using GST–Raf-RBD (lower panel; other lanes), respectively. (C) The STAT3-d358L mutant preferentially accumulated to the nucleus. 293T cells were transfected with pME/STAT3-d358L-Flag (upper panels) or pME/WT-STAT3-Flag (lower panels). After 24 h, the cells were stimulated with IL-6 for the time indicated and fixed, followed by immunostaining with the anti-p-STAT3 or anti-Flag Ab (data not shown). Bar, 10 μm. (D) STAT3-d358L constitutively bound MgcRacGAP and Rac1. Interaction of MgcRacGAP or Rac1 with WT STAT3 or STAT3-d358L was examined by coimmunoprecipitation (IP) using 293T cells transfected with either WT-STAT3 or STAT3-d358L in the absence or presence of IL-6 stimulation (upper two panels). Expression and tyrosine phosphorylation of Flag-tagged WT STAT3 or STAT3-d358L (lower two panels) were also examined.

response to G-CSF stimulation via activating SHP-2/mitogen-activated protein kinase and JAK/STAT3 pathways (10). This mutant receptor, G133, is a chimeric receptor composed of the extracellular domain of the G-CSF receptor and the transmembrane and cytoplasmic domains of gp130 truncated 133 amino acids from the transmembrane domain. Mutation of the tyrosine residue in the YXXQ motif within G133 (G133F3) abolished STAT3 activation and, thus, cell proliferation driven by G-CSF (10). G133F3 cells were transduced with the pMX-puro vector carrying the WT STAT3, STAT3C, STAT3-d358L, a constitutively active mutant H-Ras (H-RasV12), or the expression vector alone (mock). Expression levels of WT STAT3, STAT3C, and STAT3-d358L were similar as judged by Western blotting (Fig. 7B, upper panel). The expression and activation of H-RasV12 were confirmed by Western blotting (Fig. 7B, lower panel, input lane) and by a pull-down assay using GST–Raf-RBD (Fig. 7B, lower panel, other lanes), respectively. As shown in Fig. 7A, STAT3-d358L but neither WT, STAT3C, H-RasV12, nor mock treatment promoted cell proliferation of G133F3 cells under G-CSF stimulation, suggesting

that the STAT3-d358L mutant is biologically functional and could be a useful tool to study the physiological roles of STAT3 activation. This result also indicates that STAT3-d358L is stronger than STAT3C in inducing STAT3-dependent cell growth, which is consistent with their transcriptional activities (Fig. 5B).

Interestingly, the tyrosine-phosphorylated form of STAT3-d358L accumulated to the nucleus after IL-6 stimulation more evidently than that of the WT STAT3 (Fig. 7C). Importantly, the STAT3-d358L bound MgcRacGAP and Rac1 more strongly than the WT in the absence or presence of IL-6 stimulation (Fig. 7D). Although most of the phosphorylated form of overexpressed WT STAT3 remained in the cytoplasm (Fig. 7C), this was probably because p-STAT3 requires MgcRacGAP/Rac1 as cofactors to enter the nucleus and these cofactors are limiting the nuclear translocation of p-STAT3. Taken together, our results strongly indicate that the interaction of STATs with MgcRacGAP accompanied by GTP-bound Rac1 plays critical roles in regulating STAT functions through facilitating both tyrosine phosphorylation of STATs and nuclear translocation of p-STATs.

DISCUSSION

We originally identified MgcRacGAP in a search for key molecules that are involved in the IL-6-induced macrophage differentiation of M1 cells (18) and found that MgcRacGAP and Rac1 form a ternary complex with STAT3 and are required for STAT3 activation (43). We also reported that MgcRacGAP localizes to the midbody of dividing cells and plays a crucial role in the completion of cytokinesis, thus playing a distinct role in the mitotic phase (12, 33). We recently found that GTP-bound Rac1 and MgcRacGAP are required for nuclear translocation of p-STATs via the importin pathway in an in vitro nuclear transport assay (17). In this paper, to identify the molecular mechanisms of how GTP-bound Rac1 and MgcRacGAP facilitate complex formation of p-STATs with importin αs, we used MgcRacGAP conditional knockout chicken DT40 cells (5C cells) as well as a nuclear transport assay and demonstrated that the NLS of MgcRacGAP plays a critical role in the nuclear translocation of p-STAT3/5. Although the biological functions of STAT3 and STAT5 are not identical, we demonstrated that nuclear import of p-STAT3 and p-STAT5 was mediated by MgcRaGAP and its NLS, and the molecular mechanisms are common.

Liu et al. (25) reported that constitutive nuclear import of STAT3 monomer is independent of tyrosine phosphorylation and is mediated by importin α3. They found that a deletion mutant of STAT3 (d150-163) (aa 150 to 162; DVRKRVQDL EQKM) did not enter the nucleus. However, the substitution mutant of the basic amino acid cluster in this sequence did not hamper nuclear accumulation. Based on these results, they reasoned that aa 150 to 162 play a role in a conformational structure that is required for nuclear import (25). Similarly, Zeng et al. reported that aa 138 to 165 of STAT5B are required for constitutive nuclear import of STAT5B monomer but that this region does not harbor polybasic amino acids (49). Thus, it was not clear whether STAT3 and STAT5 harbor a functional NLS or whether dimer formation creates a polybasic NLS of STAT3 and STAT5. We here propose that MgcRacGAP accompanied by GTP-bound Rac1 functions as an NLS-containing nuclear chaperone toward p-STATs (Fig. 2B and C). Interestingly, Rac1 was reported to play a role in the nuclear import of SmgGDS and p120 catenin (22), members of the importin α-like armadillo family of proteins (4, 38). The C-terminal region of Rac1, but not Rac2 or Rac3, contains a polybasic region, which may function as an NLS. However, Lanning et al. (22) also suggested that the interaction of Rac1 with its GTP exchange factor SmgGDS was qualitatively different from that of NLS-containing molecules with importin αs. Consistent with this, we failed to detect direct interactions of GTP-bound Rac1 with importin αs in either the in vitro binding assay or yeast two-hybrid assay (data not shown). Therefore, it is unlikely that GTP-bound Rac1 serves directly as an NLS-containing chaperone of p-STATs. The results shown in Fig. 2C strongly indicate that GTP-bound Rac1 activates the NLS MgcRacGAP associating with p-STATs; however, the precise molecular mechanism for the requirement of Rac1 remains to be clarified by structural analysis.

The present results demonstrate that the bipartite NLS (182KRR/199KK) of MgcRacGAP is essential for the nuclear transport and the transcriptional activation of p-STATs in living cells (Fig. 3G and H and 4A). The results of the nuclear-cytosol fractionation analysis using the 5C cells expressing 199AA and 182AAA/199AA (Fig. 3G) also suggested that the preferential nuclear localization of MgcRacGAP is mediated by the importin pathway in living cells. However, in the nuclear transport assay using semi-intact cells and purified proteins, nuclear translocation of MgcRacGAP was not achieved by the addition of importin α/β pathway proteins alone and, interestingly, further addition of p-STATs and GTP-bound Rac1 was required for nuclear translocation of MgcRacGAP (see Fig. S3A and B in the supplemental material). This raised a question of why overexpressed MgcRacGAP predominantly accumulated to the nucleus in HeLa cells, where STATs were not extensively activated. In addition, purified MgcRacGAP pulled down importin αs from the HeLa cell lysate (see Fig. S1B in the supplemental material), while it did not bind purified importin αs in the in vitro binding assay (Fig. 2C and data not shown). These results suggest that the NLS of MgcRacGAP can be activated by other cargo proteins as well as by p-STAT and GTP-bound Rac1. Thus, MgcRacGAP may function as a nuclear chaperone for not only p-STATs but also another nuclear protein(s).

The conditional knockout of MgcRacGAP in 5C cells decreased the G-CSF-induced tyrosine phosphorylation of STAT3 (Fig. 3C), and small interfering RNA-mediated MgcRacGAP knockdown in Ba/F3 cells also reduced tyrosine phosphorylation of STAT5 (17). These results implied that MgcRacGAP functions as an upstream regulator of STAT activation as well. In relation to this, STAT mutants harboring deletions in the βb-βc loop showed enhanced interaction with MgcRacGAP and became constitutively active (Fig. 5 and 6). It should be noted that the extent of tyrosine phosphorylation of STAT3-d358L without stimulation was weaker than that of WT 16 h after IL-6 stimulation (Fig. 7D), although the association of STAT3-d358L with MgcRacGAP/Rac1 was stronger than that of WT under the same conditions (Fig. 5C and 7D). These results indicate that the stronger association of the constitutively active STAT mutants with MgcRacGAP was not a